Contents list available at CBIORE journal website

International Journal of Renewable Energy Development

Journal homepage: https://ijred.cbiore.id

/Research Article

Identification and comparison of pyrolysis products of different biomasses from agro-industrial using TGA-FTIR and Py-GC/MS

Marco Rosero Espín[a*], Morayma Angelica Muñoz Borja[b,c], Ricardo Narvaez Cueva[a], Boris German Insuasti[d], Sebastián Espinoza[b], Angela N. Garcia Cortés[c], Antonio Marcilla[c]

[a] *Faculty of Chemical Engineering, Central University of Ecuador, Quito, Ecuador*

[b] *Geological and Energy Research Institute, Quito, Ecuador.*

[c] *Department of Chemical Engineering, Alicante University, San Vicente del Raspeig, España*

[d] *Empresa Pública de Hidrocarburos EP PETROECUADOR, Quito-Ecuador*

Abstract. The valorization of agro-industrial residues is crucial for the circular bioeconomy. This study elucidates the thermal decomposition mechanisms and volatile product distribution of four distinct Ecuadorian biomasses: balsa wood (Bl), sugarcane bagasse (Bg), cocoa husks (Cc), and coffee husks (Cf), TGA kinetics. TGA and DTG profiles showed the characteristic multistage degradation of lignocellulosic materials, with maximum mass-loss rates occurring between 320 and 360 °C depending on the biomass. Bl and Bg, which contained the highest cellulose fractions (33–35%), exhibited sharp DTG peaks and higher decomposition temperatures. In contrast, Cc and Cf, both lignin-rich residues (up to 42–47%)—displayed broader degradation profiles, delayed devolatilization, and higher char yields (>26%). Kinetic evaluation confirmed these trends, with cellulose-rich samples showing higher activation energies than lignin-dominated husks. The in-situ FTIR monitoring revealed clear compositional differences in evolved gases: Bl and Bg generated higher proportions of CO and carbonyl-containing volatiles, whereas Cc and Cf produced more CO_2 and phenolic signals associated with lignin fragmentation. Py-GC/MS supported these observations, identifying dominant aldehydes and alcohols in Bl and Bg, while Cc and Cf produced elevated levels of phenols, guaiacols, and nitrogenous aromatics. Overall, the integration of TGA–FTIR and Py-GC/MS allowed establishing direct correlations between lignocellulosic composition, kinetic parameters, and volatile speciation. Unlike previous studies that report either kinetic parameters or volatile fingerprints separately, this work establishes direct kinetic–molecular correlations between activation energy domains and dominant volatile families for Ecuadorian biomasses. The results indicate that balsa wood is a promising feedstock for generating oxygenated chemical intermediates, whereas coffee husk shows strong potential for biochar-oriented processes due to its high lignin content and char yield. These findings expand the thermochemical characterization of Ecuadorian agro-industrial residues and support their selective valorization through pyrolysis.

Keywords: Agro-industrial residues, Pyrolysis, Volatile products, TG, FTIR and GCMS

@ The author(s). Published by CBIORE. This is an open access article under the CC BY-SA license (http://creativecommons.org/licenses/by-sa/4.0/).

Received: 23rd Sept 2025; Revised: 16th Dec 2025; Accepted: 15th January 2026; Available online: 27th January 2026

1. Introduction

The exponential growth of the agro-industrial sector in tropical regions like Ecuador generates vast quantities of lignocellulosic residues, often discarded without adequate valorization strategies. This accumulation not only represents a loss of potential energy but also poses severe environmental risks, including greenhouse gas emissions from uncontrolled decomposition. In this context, the transition from a linear disposal model to a circular bioeconomy.

Ecuador has a wide and diverse agricultural production across its different regions, which generates a significant amount of organic matter (biomass) waste. Much of this biomass is discarded without adequate final disposal, causing environmental degradation through the accumulation of waste in open areas. Therefore, the integral utilization of agricultural residues for energy purposes represents an opportunity to stimulate socioeconomic development in the rural areas.

Residual biomass refers to by-products derived from agricultural, livestock, human, and forestry activities (de Lucas Herguedas & Rodríguez García, 2012). The characteristics of biomass vary depending on factors such as soil composition, plant species, and topography. Biomass of plant origin is primarily composed of lignocellulosic structures, including cellulose, hemicellulose, and lignin, along with small amounts of extractives (Ge, *et al.*, 2018). he typical weight percentage distribution of hemicellulose, cellulose, and lignin varies by species, generally ranging between 15–30%, 40–60%, and 10–30%, respectively.

The Bioenergetic Atlas of Ecuador, published by the Coordinating Ministry of Production, Employment, and Competitiveness (MCPEC), provides valuable data on the main biomasses generated by the agricultural sector, such as rice, bananas, cocoa, coffee, sugarcane, hard corn, African palm, heart of palm, pineapple, and plantains. According to this document, African palm generates approximately 6.9 million

* Corresponding author
Email: mvrosero@uce.edu.ec (M. R. Espín)

https://doi.org/10.61435/ijred.2026.61812
ISSN: 2252-4940/© 2026.The Author(s). Published by CBIORE

tons of waste per year (equivalent to the energy contained in 653 million gallons of diesel), while cocoa produces about 2 million tons annually (equivalent to 101 million gallons of diesel) (ESIN Consultora S.A., 2014) (Reed & Siddhartha, 1994).

Among the alternative technologies for managing solid waste, thermal processes such as pyrolysis offer promising technological advantages. Pyrolysis is a complex physicochemical process that enables the energetic recovery of biomass by decomposing organic matter at various temperature ranges under limited or complete absence of oxygen, producing hydrocarbon liquids (bio-oil), combustible gases (biogas), and solid residues (biochar) (Fagbemi, 2001). This study focuses on the identification and comparison of volatile pyrolysis products obtained from the transformation of residual biomass generated in the agro-industrial sector, specifically cocoa husks, coffee husks, sugarcane bagasse, and balsa wood. These biomasses exhibit significant potential for conversion into energy carriers or value-added chemical feedstocks.

Previous studies have reported that slow pyrolysis of cocoa biomass yields a complex oily fraction containing families of ketones such as hydroxyketones, aliphatic ketones, and cyclic ketones, as well as aldehydes, furans, phenols, alkylphenols, alkylbenzenes, and other chemical compounds (Mansur, 2014). In the case of coffee biomass, the pyrolysis mechanisms of lignin are notably more complex than those of cellulose and hemicellulose. Lignin undergoes primary degradation reactions between 200 °C and 400 °C, followed by secondary reactions above 400 °C. Hemicellulose decomposes mainly between 200 °C and 400 °C, while cellulose degradation occurs between 315 °C and 400 °C. These decomposition pathways contribute to pyrolytic polymerization reactions, leading to the formation of biochar and activated carbon precursors (Reis, 2020) (Changjuna, 2014).

The thermochemical conversion of sugarcane bagasse by slow pyrolysis generates a wide variety of volatile condensable compounds, including those by Dellrose, *et al*, (2021) and Muñoz *et al*. (2024), have identified key families of compounds derived from the thermal degradation of lignocellulosic structures. Table 1 presents a summary of the most relevant volatile compounds detected during the slow pyrolysis of sugarcane bagasse, integrating findings from both references. The identified products mainly include organic acids, furan derivatives, phenolic compounds, and carbonyl species, all of which are associated with the decomposition of cellulose, hemicellulose, and lignin components. Thermochemical conversion processes, particularly pyrolysis, have garnered significant attention from the scientific community due to their versatility as both intermediate stages of various thermal treatments and as direct routes for the production of high-quality fuels (Dick, 2020) (Dhyani & Bhaskar, 2019). This methodology has opened numerous opportunities for the beneficial utilization of biomass, broadly referring to all organic materials of plant origin (Wang G. Y., 2020) (Gogoi, 2023).

The energetic and chemical valorization of Ecuadorian biomass through pyrolysis offers a promising alternative for sustainable management of agricultural residues. By characterizing the volatile compounds produced from the thermal decomposition of cacao husks, coffee husks, sugarcane bagasse, and balsa wood, this study provides insights into their degradation pathways and potential applications. The identification of key volatile compounds supports the development of integrated biorefinery strategies aimed at energy production and the synthesis of high-value chemical intermediates, contributing to a circular bioeconomy.

2. Materials and Methods

2.1. Biomass Used

This study employed four types of biomasses: balsa wood (Bl), sugarcane bagasse (Bg), cocoa husks (Cc), and coffee husks (Cf). All samples were sourced directly from post-harvest agricultural processes, representing typical residues from Ecuadorian agro-industrial activities. The balsa wood biomass (*Ochroma pyramidale*) was collected from commercial plantations located in the canton of Mocache, province of Los Ríos, Ecuador. The wood samples corresponded to trees approximately four years old, harvested between 2018 and 2021, and originated from native species cultivated for commercial purposes. The initial moisture content of the balsa samples was approximately 11%. The sugarcane bagasse (Saccharum officinarum) was obtained from local "trapiches" in Quito, Ecuador, as a by-product of guarapo juice extraction for alcoholic fermentation processes. The collected bagasse presented an initial moisture content of approximately 8.4%.

The cocoa husks (*Theobroma cacao* L.) were sourced from a national fine aroma cocoa plantation located in the province of Los Ríos. The harvest, carried out between June and August 2018, was carefully selected to include only native Ecuadorian varieties, avoiding any mixing with CCN-51 cocoa. Samples were collected on a wet basis immediately after the post-harvest process, presenting a moisture content of approximately 10%. The coffee husks (*Coffea arabica*) were obtained from the post-harvest processing of roasted coffee beans between 2020 and 2021, also from plantations in Mocache, Los Ríos province. The coffee husk samples exhibited a moisture content of approximately 9%.

2.1. Pretreatment

Prior to characterization and experimental procedures, all biomass samples were subjected to natural drying under

Table 1
Volatile condensable compounds identified from bagasse pyrolysis.

Family	Compound	Representative Function
Organic acids	Acetic acid	Product of hemicellulose deacetylation
	Propanoic acid	Minor degradation of sugars
Furans and derivatives	2-Furancarboxaldehyde (Furfural)	Marker of pentosan degradation
	5-Hydroxymethyl-2-furancarboxaldehyde (HMF)	Derived from hexose dehydration
	5-Methyl-2-furancarboxaldehyde	Secondary furan derivative
Phenolic compounds	Phenol	Primary lignin degradation product
	Eugenol	Lignin-derived with aromatic and allyl structures
	2-Methoxy-4-(1-propenyl)phenol (Isoeugenol)	Phenolic compound from lignin
	4-Ethyl-2-methoxyphenol	Guaiacol derivative from lignin
	2,6-Dimethoxyphenol (Syringol)	Typical marker of syringyl lignin units
Carbonyl compounds	1-(2-Furanyl)ethanone	Furanone derivative
	Maltol	Sugar decomposition product
	Vanillic acid	Oxidized lignin derivative

ambient conditions (23 °C, 0.71 bar, and 60% relative humidity) for three days. Subsequently, the materials were milled using a Retsch SM300 cutting mill and sieved with a Syntron mechanical system. Mesh sizes No. 35 (0.5 mm), No. 60 (0.25 mm), No. 120 (0.125 mm), and No. 230 (0.063 mm) were employed, with only the fraction retained on the No. 35 sieve (0.5 mm) selected for further analysis.

2.1. Methods

2.3.1. Elemental analysis

The elemental analysis was performed using an Elementar Vario Macro Cube analyzer at the Research Services Laboratory of the Central University of Ecuador. The test is based on the DUMAS method, in which the sample undergoes instant combustion with pure oxygen at a temperature above 1000 °C. During combustion, carbon is oxidized to carbon dioxide (CO_2), hydrogen to water (H_2O), and sulfur to sulfur dioxide (SO_2). Nitrogen oxides formed during the process are subsequently reduced to elemental nitrogen gas (N_2) in a reduction furnace. T precise determination of carbon, hydrogen, nitrogen, and sulfur contents in the biomass samples.

2.3.2. Thermogravimetric Analysis (TGA)

Thermogravimetric analysis (TGA) is a widely employed technique for studying the decomposition reactions of various materials, providing insights into their thermal behavior, the determination of kinetic parameters, and the influence of temperature and heating rate on the development of decomposition mechanisms (Cutiño, 2011). TGA also allows for the assessment of the chemical and physical properties of char materials (Li, 2014). Thermogravimetric analysis (TGA) was conducted to study the thermal decomposition behavior of the biomasses and to determine key decomposition parameters under controlled conditions. TGA experiments were performed using a METTLER TOLEDO TGA/DSC1 STAR System analyzer. Approximately 6 mg of each biomass sample (balsa wood, sugarcane bagasse, cocoa husks, and coffee husks) were weighed into pre-tared silicon oxide crucibles. The samples were heated at a slow heating rate of 20 °C min^{-1} from 25 °C to 700 °C under a constant nitrogen flow of 80 mL min^{-1} to maintain an inert atmosphere. Each test was performed in duplicate to verify the reproducibility of the results. The thermogravimetric curves obtained were analyzed to study the different decomposition stages, evaluate mass loss profiles, and support kinetic modeling of the pyrolysis behavior of the biomasses.

The kinetic analysis was performed to describe the thermal degradation behavior of the agro-industrial biomasses under non-isothermal conditions. The procedure combined both model-fitting and isoconversional approaches to obtain reliable activation energies and kinetic parameters for each decomposition stage. Thermogravimetric (TG) and derivative thermogravimetric (DTG) data were obtained under an inert helium atmosphere at four heating rates (5, 10, 20, and 30 °C·min^{-1}).

The mass-loss (w) and rate (dw/dt) curves were recorded from 30 °C to 800 °C. Before kinetic analysis, experimental data were smoothed and normalized to a dimensionless conversion degree α, defined as:

$$\boldsymbol{\alpha = \frac{w_0 - w_t}{w_0 - w_f}} \quad (1)$$

Where w_0, w_t and w_f represent the initial, instantaneous, and final mass of the sample, respectively. The kinetic analysis was performed using the Independent Parallel Reaction (IPR) model, which assumes that the overall rate of mass loss is a linear combination of the decomposition rates of the three major pseudo-components: hemicellulose, cellulose, and lignin7. This approach allows for the deconvolution of the DTG curves into individual Gaussian peaks, providing specific kinetic triplets for each biomass constituent.

2.3.3. FTIR Infrared Spectroscopy

Fourier Transform Infrared (FTIR) spectroscopy was used to analyze the chemical composition and optical properties of volatile products released during the thermal decomposition of biomass (Bassilakis, 2001) (Li, 2014). This technique is essential for the identification of functional groups associated with the evolved gases, providing key insights into the decomposition mechanisms during pyrolysis.

The analysis was carried out using a Bruker Tensor 27 FTIR spectrometer connected online to the thermogravimetric analyzer (TGA) via a heated transfer line maintained at 230 °C to prevent condensation. Approximately 6 mg of biomass were placed in a silicon oxide crucible. The thermal decomposition was performed in a nitrogen atmosphere (80 mL min^{-1}) over a temperature range from 25 °C to 700 °C at a constant heating rate of 20 °C min^{-1}. the analysis was recorded within an infrared range of 600–4000 cm^{-1}, with a spectral resolution of 4 cm^{-1}. A total of 200 and 100 scans were performed for the background and the sample spectra, respectively. Due to the gas residence time in the transfer line and the filling time of the spectrometer's optical cell, a start-time delay of approximately 3 minutes was observed between TGA and FTIR data acquisition.

2.3.4. Analytical pyrolysis (Py- GC/MS)

Analytical pyrolysis coupled with gas chromatography–mass spectrometry (Py-GC/MS) was employed to characterize the thermal degradation products of the biomass samples (Huertas, 2022) (Ma, 2014). This highly sensitive technique decomposes the biomass into smaller stable fragments (pyrolysates), which are then analyzed to identify the primary volatile compounds.

The analysis was performed on a Multi-Shot-Pyrolyzer EGA/PY 3030D connected in-line with a gas chromatograph with mass spectrometry detector (EGA-GC/MS). The pyrolyzer consists of a ceramic furnace capable of heating up to 1050 °C, with the insertion of the sample in free fall into a quartz tube. Pyrolysis tests were carried out under six different temperatures of 450, 550, 650, 750, 850 °C. During the pyrolysis time, the gases generated in the furnace are sucked through an interface heated to 300 °C to the gas chromatograph (GC) model Agilent 6890B coupled to a mass spectrometer (MS) model Agilent 5973 MSD. The mass spectrometer has a transmission quadrupole for qualitative and quantitative analysis by electronic ionization (EI), positive chemical ionization (PCI), and negative chemical ionization (NCI). A sample quantity (approximately 0.11 mg) was placed in a metal sample holder, which was then inserted into the quartz reactor. The oven was preheated to the selected operating temperature, and analytical pyrolysis of the sample was performed. The volatile compounds released during 12 seconds were fed into the GC.

The objective of the Py-GC/MS experiments was to obtain molecular-level fingerprints of the volatile fraction under well-controlled analytical conditions. Therefore, this study does not aim to quantify bio-oil, gas, or char yields, which require reactor-scale experiments. Instead, the focus is placed on establishing structure–reactivity relationships between lignocellulosic composition, kinetic parameters, and volatile speciation.

The set of columns used was HP-5MS UI (30 m x 250 µm x 0.25 µm) (5%-phenyl)-methylpolysiloxane in phase and the selected operating conditions were: helium flow in the column: 2 mL min−1, injection mode: split (1:50), injector temperature: 280 °C, initial furnace temperature: 45 °C by 5 min, heating rate: 12 °Cmin-1 and final oven temperature: 285 °C per 10 min.

3. Results and Discussion

3.1. Characterization of biomasses

The four selected raw materials balsa wood (Bl), sugarcane bagasse (Bg), cocoa husk (Cc), and coffee husk (Cf) are lignocellulosic residues that exhibit comparable carbon and hydrogen contents, ranging from approximately 41% to 50% C and 5.3% to 6.2% H, as shown in Table 1. Oxygen content varies between 43.1% and 51.7%, while nitrogen content shows more marked differences among the biomasses: balsa wood and bagasse present low nitrogen contents (0.14–0.21%), whereas cocoa and coffee husks exhibit higher values, with coffee husk reaching 2.39%, likely due to the presence of nitrogenous compounds such as caffeine.

Moisture contents after sample conditioning also differed. Balsa wood and cocoa husk exhibited relatively lower moisture levels (10.3% and 12.8%, respectively), while sugarcane bagasse and coffee husk had higher values (13.1% and 14.8%, respectively). These differences are attributed to intrinsic properties of each biomass, their botanical origin, and the specific conditions of harvest and sample preparation. In the case of cocoa biomass, although moisture values from the literature mainly refer to the cocoa shell (6.7–7.4%) (Sangronis, 2014) (Ortiz de Bertorelli, 2004), there are no specific bibliographic values for the Ecuadorian native cocoa husk used in this study. Therefore, the observed moisture content is considered acceptable within typical variability ranges.

Additionally, published moisture contents for other lignocellulosic residues are consistent with our results, with balsa wood around 12% (Moncayoa, 2018), sugarcane bagasse near 16% (Ouedraogo, 2022), and coffee husk between 10.1–12% (Manals, 2018), (Patiño-Velasco, 2016). Variations can arise due to differences in species, climatic conditions, and drying protocols.

3.2. Thermal decomposition (TGA / DTG)

Figures 1 show the thermogravimetric (TG) and derivative thermogravimetric (DTG) curves of the studied biomasses: balsa wood, sugarcane bagasse, cocoa hulls, and coffee husks. The DTG curves were obtained by deriving the TG curves. Thermogravimetric (TG) (a) and derivative thermogravimetric (DTG) (b) curves of the studied biomass samples: Balsa wood (Bl), sugarcane bagasse (Bg), cocoa husk (Ca), coffee husk (Cc).

Differences and similarities in the composition, commented on in the previous section, are clearly shown in these curves, being able to observe a greater parallelism between the decomposition of the balsa and bagasse samples,

Table 2
Initial characterization of biomasses

	Elemental Analysis					Moisture content (%)		
	C	H	O	N	S	Experimental value	Bibliographic value	Reference
Bl	49,5	6,20	44,2	0,14	0,0	10,3	12	(Moncayoa, 2018)
Bg	47,6	6,07	46,1	0,21	0,0	13,1	16,07	(Manals-Cutiño, 2015) (Ouedraogo, 2022)
Cc	41,1	5,38	51,7	1,80	0,0	12,8	6,7- 7,41	(Sangronis, 2014), (Ortiz de Bertorelli, 2004)
Cf	48,3	6,17	43,1	2,39	0,0	14,8	10,1 – 12	(Manals, 2018), (Patiño-Velasco, 2016)

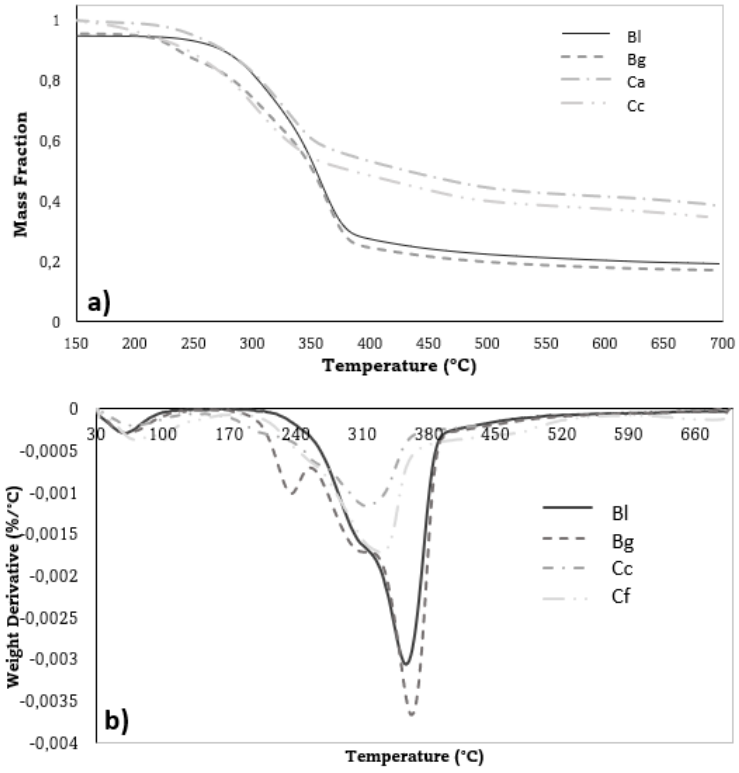

Fig. 1 Thermogravimetric (TG) (a) and derivative thermogravimetric (DTG) (b) curves of the studied biomass samples: Balsa wood (Bl), sugarcane bagasse (Bg), cocoa husk (Ca), coffee husk (Cc).

on the one hand, and between those of cocoa and coffee residues on the other.

The TG curves reveal the overall thermal stability and decomposition profiles of the biomasses. Balsa wood and sugarcane bagasse exhibit similar thermal behavior, characterized by a sharp weight loss associated with cellulose degradation and relatively low final residue percentages (approximately 17%). In contrast, cocoa and coffee husks show higher final residue values (23–24%), indicating a greater lignin content, as lignin is known to contribute to higher char yields during pyrolysis (Raveendran *et al*., 1996). This is consistent with the compositional differences discussed previously, where balsa and bagasse showed higher cellulose proportions, while cocoa and coffee husks contained larger fractions of lignin and hemicellulose (Raveendran, Pyrolysis characteristics of biomass and biomass components, 1996).

The DTG curves provide more detailed insights into the decomposition mechanisms of the biomasses. At temperatures below 100 °C, all samples exhibit an initial weight loss attributed to moisture evaporation. Additionally, a small, sharp peak around 100 °C is observed in the cocoa and coffee husk samples, which can be attributed to the volatilization of light extractives, as previously described in studies on cocoa and coffee processing residues (Aleida, 2018) (Poyilil, 2022).

In the case of sugarcane bagasse, a distinct DTG peak appears at approximately 229 °C, likely corresponding to the thermal decomposition of residual sucrose, a characteristic feature of this biomass (Wang *et al*., 2018). Following this, between 250 and 550 °C, the main decomposition events occur, associated with the breakdown of hemicellulose, cellulose, and lignin fractions. Balsa wood and sugarcane bagasse show a main DTG peak centered around 360 °C, which is primarily attributed to cellulose decomposition, with a minor shoulder at approximately 310 °C linked to hemicellulose degradation. Above 400 °C, a gradual weight loss is observed, related to the progressive degradation of lignin, as typically reported for lignocellulosic materials (Manals-Cutiño, 2015) (Yang H. &., 2007).

Cocoa and coffee husks, however, display a different decomposition profile. The main DTG peaks for these biomasses occur at lower temperatures, around 320–330 °C, indicating a significant contribution of hemicellulose to the thermal degradation process. Additionally, a broad shoulder is observed between 400–500 °C, reflecting a substantial lignin fraction decomposing over a wide temperature range, which aligns with previous observations for these agricultural residues (Biagini, 2006) (Liu Q., 2020). At temperatures above 600 °C, both cocoa and coffee husks present minor but broad DTG peaks, suggesting the decomposition of inorganic compounds, such as carbonates, corroborating their higher ash content as discussed in the initial characterization.

Overall, the thermal decomposition behavior of the biomasses correlates well with their lignocellulosic composition. Balsa wood and sugarcane bagasse, with their higher cellulose content and lower lignin fraction, exhibit sharper and more defined thermal decomposition peaks at higher temperatures. In contrast, cocoa and coffee husks, with higher lignin and hemicellulose contents, show broader degradation events at slightly lower temperatures and higher residual masses after pyrolysis.

Table 3 summarizes the main thermal events identified for each biomass, providing an overview of the decomposition stages related to moisture loss, extractives release, hemicellulose, cellulose, and lignin degradation. These observations are consistent with the thermal degradation mechanisms described in the literature for similar lignocellulosic materials (Saldarriaga, *et al*., 2015) (Raveendran, Pyrolysis characteristics of biomass and biomass components, 1996). Differences and similarities in the composition, commented on in the previous section, are clearly shown in these curves, being able to observe a greater parallelism between the decomposition of the balsa and bagasse samples, on the one hand, and between those of cocoa and coffee residues on the other.

The TG curves reveal the overall thermal stability and decomposition profiles of the biomasses. Balsa wood and sugarcane bagasse exhibit similar thermal behavior, characterized by a sharp weight loss associated with cellulose degradation and relatively low final residue percentages (approximately 17%). In contrast, cocoa and coffee husks show higher final residue values (23–24%), indicating a greater lignin content, as lignin is known to contribute to higher char yields

Table 3
Thermal events and percentage of weight loss of balsa residues, sugarcane bagasse, cocoa, and coffee husk analyzed by TGA.

Biomasses	Zone	Thermal event	Temperature Range (°C)
Bl	1	Water loss	< 110
	2	volatiles decomposition	110 - 190
	3	hemicellulose decomposition	190 - 300
	4	Cellulose decomposition	300 - 550
	5	Lignin decomposition	> 550
BG	1	Water loss	< 110
	2	volatiles decomposition	110 - 190
	3	hemicellulose decomposition	190 - 300
	4	Cellulose decomposition	300 - 550
	5	Lignin decomposition	> 550
Cc	1	Water loss	< 110
	2	volatiles decomposition	110 - 210
	3	hemicellulose decomposition	210 – 280
	4	Cellulose decomposition	280 – 380
	5	Lignin decomposition	> 380
Cf	1	Water loss	< 110
	2	volatiles decomposition	110 - 210
	3	hemicellulose decomposition	210 - 280
	4	Cellulose decomposition	280 – 380
	5	Lignin decomposition	> 380

during pyrolysis (Raveendran *et al*., 1996). This is consistent with the compositional differences discussed previously, where balsa and bagasse showed higher cellulose proportions, while cocoa and coffee husks contained larger fractions of lignin and hemicellulose (Raveendran, Pyrolysis characteristics of biomass and biomass components, 1996).

The DTG curves provide more detailed insights into the decomposition mechanisms of the biomasses. At temperatures below 100 °C, all samples exhibit an initial weight loss attributed to moisture evaporation. Additionally, a small, sharp peak around 100 °C is observed in the cocoa and coffee husk samples, which can be attributed to the volatilization of light extractives, as previously described in studies on cocoa and coffee processing residues (Aleida, 2018) (Poyilil, 2022).

In the case of sugarcane bagasse, a distinct DTG peak appears at approximately 229 °C, likely corresponding to the thermal decomposition of residual sucrose, a characteristic feature of this biomass (Wang *et al*., 2018). Following this, between 250 and 550 °C, the main decomposition events occur, associated with the breakdown of hemicellulose, cellulose, and lignin fractions. Balsa wood and sugarcane bagasse show a main DTG peak centered around 360 °C, which is primarily attributed to cellulose decomposition, with a minor shoulder at approximately 310 °C linked to hemicellulose degradation. Above 400 °C, a gradual weight loss is observed, related to the progressive degradation of lignin, as typically reported for lignocellulosic materials (Manals-Cutiño, 2015) (Yang H. &., 2007).

Cocoa and coffee husks, however, display a different decomposition profile. The main DTG peaks for these biomasses occur at lower temperatures, around 320–330 °C, indicating a significant contribution of hemicellulose to the thermal degradation process. Additionally, a broad shoulder is observed between 400–500 °C, reflecting a substantial lignin fraction decomposing over a wide temperature range, which aligns with previous observations for these agricultural residues (Biagini, 2006) (Liu Q., 2020). At temperatures above 600 °C, both cocoa and coffee husks present minor but broad DTG peaks, suggesting the decomposition of inorganic compounds, such as carbonates, corroborating their higher ash content as discussed in the initial characterization.

Overall, the thermal decomposition behavior of the biomasses correlates well with their lignocellulosic composition. Balsa wood and sugarcane bagasse, with their higher cellulose content and lower lignin fraction, exhibit sharper and more defined thermal decomposition peaks at higher temperatures. In contrast, cocoa and coffee husks, with higher lignin and hemicellulose contents, show broader degradation events at slightly lower temperatures and higher residual masses after pyrolysis.

Table 3 summarizes the main thermal events identified for each biomass, providing an overview of the decomposition stages related to moisture loss, extractives release, hemicellulose, cellulose, and lignin degradation. These observations are consistent with the thermal degradation mechanisms described in the literature for similar lignocellulosic materials (Saldarriaga, *et al*., 2015) (Raveendran, Pyrolysis characteristics of biomass and biomass components, 1996).

3.3.1. Mandar Kinetic study

The thermal decomposition behavior of lignocellulosic biomass was modeled using an Independent Parallel Reaction (IPR) scheme, where each pseudo-component hemicellulose, cellulose, lignin, and an additional residual fraction decomposes independently within a specific temperature range. This model effectively describes the overlapping decomposition stages typically observed in DTG curves of lignocellulosic materials (Molto, 2011; Siddiqi H. &., 2020).

The overall mass loss is then expressed as the sum of the individual contributions of these pseudo-components (Siddiqi H. &., 2020; Munoz, 2024), each governed by an Arrhenius-type rate law of n-th order

$$-\frac{dw_i}{dt} = k_{o,i} e^{\left(-\frac{E_{a,i}}{RT}\right)} w_i^{n_i} \qquad (2)$$

where $w_i$is the remaining mass fraction, $k_{o,i}$ (s^{-1}) the pre-exponential factor, $E_{a,i}$ ($kJ \cdot mol^{-1}$) the activation energy, $R$the gas constant, T the absolute temperature, and n_i the apparent order. The global rate is the weighted sum:

$$\left(\frac{dw}{dt}\right)_{cal} = \sum_{i}^{4} y_i \, k_{o,i} e^{\left(-\frac{E_{a,i}}{RT}\right)} w_i^{n_i} \qquad (3)$$

with y_i the mass fraction of each pseudo-component. Parameters $(A_i, E_{a,i}, n_i, y_i)$ were estimated by minimizing a joint objective function that balances TG and DTG deviations:

$$OF = \sum_{t} \left[\left(w_{exp,t} - w_{cal,t}\right)^2 + \lambda \left(\left(\frac{dw}{dt}\right)_{exp,t} - \left(\frac{dw}{dt}\right)_{cal,t} \right)^2 \right] \qquad (4)$$

The weighting factor λ was adjusted so that both TG and DTG curves were equally represented in the fitting. This approach allows accurate reproduction of the full DTG curve shape main peaks and shoulders while maintaining fidelity to overall mass balance.

As done by (Munoz, 2024)**,** for bagasse. This ensures that peak positions/heights (DTG) and overall mass balance (TG) are simultaneously reproduced. A small global correction factor β was used per heating rate to absorb instrumental/sample dispersion without altering the physical meaning of the kinetic parameters consistent with prior practice.

The values (Ea, k0, n) are the result of models that seek to simulate the complex decomposition processes of lignocellulosic biomass, allowing the degradation processes to be modeled based on thermogravimetric data (Siddiqi H. &., 2020; White, 2011). Biomass residues (balsa, bagasse, cocoa, and coffee) are composed of hemicellulose, cellulose, and lignin. The four pseudo-components (W1, W2, W3, W4) modeled in their study generally attempt to reflect the decomposition of these main fractions (TranVan, 2014).

The kinetic parameters obtained for balsa and cocoa husk residues (Table 4) fall within the typical ranges reported in the literature for lignocellulosic materials (Raveendran & col., Pyrolysis characteristics of biomass and biomass components, 1996; Garrido, Font, & Conesa, 2016; Yang & col., 2019). Apparent activation energies ranged from 70–150 $kJ \cdot mol^{-1}$ for hemicellulose and cellulose fractions, up to 300 $kJ \cdot mol^{-1}$ for lignin.

It must be emphasized that the activation energies reported here are apparent parameters derived from a lumped kinetic model and do not represent single elementary reactions, but rather the cumulative energetic barriers of overlapping devolatilization, condensation and char-forming processes. Balsa wood (Bl) and sugarcane bagasse (Bg), typically rich in holocellulose (cellulose + hemicellulose), often exhibit a main stage of high activation energy corresponding to cellulose (Salazar & Aburto, 2015; Rezende, 2011; Mahmuda, 2021).

For Bl, the decomposition is governed by two dominant fractions. The first, W_1, presents an activation energy of 241.6 $kJ \cdot mol^{-1}$, typical of the cellulosic domain that decomposes between 315–400 °C. Similar ranges (200–250 $kJ \cdot mol^{-1}$) were

Table 4
Kinetic parameters adjusted for the biomasses studied

Biomasses	Parameter	W1	W2	W3	W4
Bl	E/R	29,057.23	8,780.83	56,281.59	12,346.80
	k_0 [s^{-1}]	$5.481 \cdot 10^{23}$	$4.789 \cdot 10^{3}$	$1{,}565 \cdot 10^{38}$	$1.991 \cdot 10^{36}$
	E_a [kJmol^{-1}]	241,58	73	467.92	100.43
	n	1.35	0.57	1.71	3.04
	FO		0.0201		
Bg	E/R	29,057.23	36,558.30	5,980.37	6,661.88
	k_0 [s^{-1}]	$5.258 \cdot 10^{23}$	$3.847 \cdot 10^{23}$	35.313	50.876
	E_a [kJmol^{-1}]	129.2	117.4	213.8	202.4
	n	1.36	1.15	0.357	1.79
	FO		0.00799		
Cc	E/R	9,743.86	39,817.19	5,407,22	3881,15
	k_0 [s^{-1}]	$1.658 \cdot 10^{12}$	$1.12 \cdot 10^{28}$	19.02	0.30
	E_a [kJmol^{-1}]	79,26	323,87	43.98	31,56
	n	0.65			
	FO		0.0106		
Cf	E/R	9,743,87	7,466.71	8,075.96	4,476.54
	k_0 [s^{-1}]	$1.68 \cdot 10^{12}$	620.879	2,386.151	0.7128
	E_a [kJmol^{-1}]	1,171.98	898.09	971.37	538.43
	n	3.24	0.94	0.58	1.01
	FO		0.00959		

reported by (TranVan, 2014) and (Raveendran, Pyrolysis characteristics of biomass and biomass components, 1996) for crystalline cellulose. The second event (73 kJ·mol^{-1}) corresponds to the lignin-associated fraction, which initiates degradation at lower temperatures and over broader intervals due to its heterogeneous aromatic network. The remarkably high E_a observed for W_3 in Balsa (467.9 kJ·mol^{-1}) likely represents secondary cracking or condensation reactions producing char at advanced stages, as observed in distributed kinetic models of complex systems (Molto, 2011; Ríos, 2013).

For Bg, intermediate activation energies (117–129 kJ·mol^{-1}) were obtained for W_1–W_2, consistent with hemicellulose

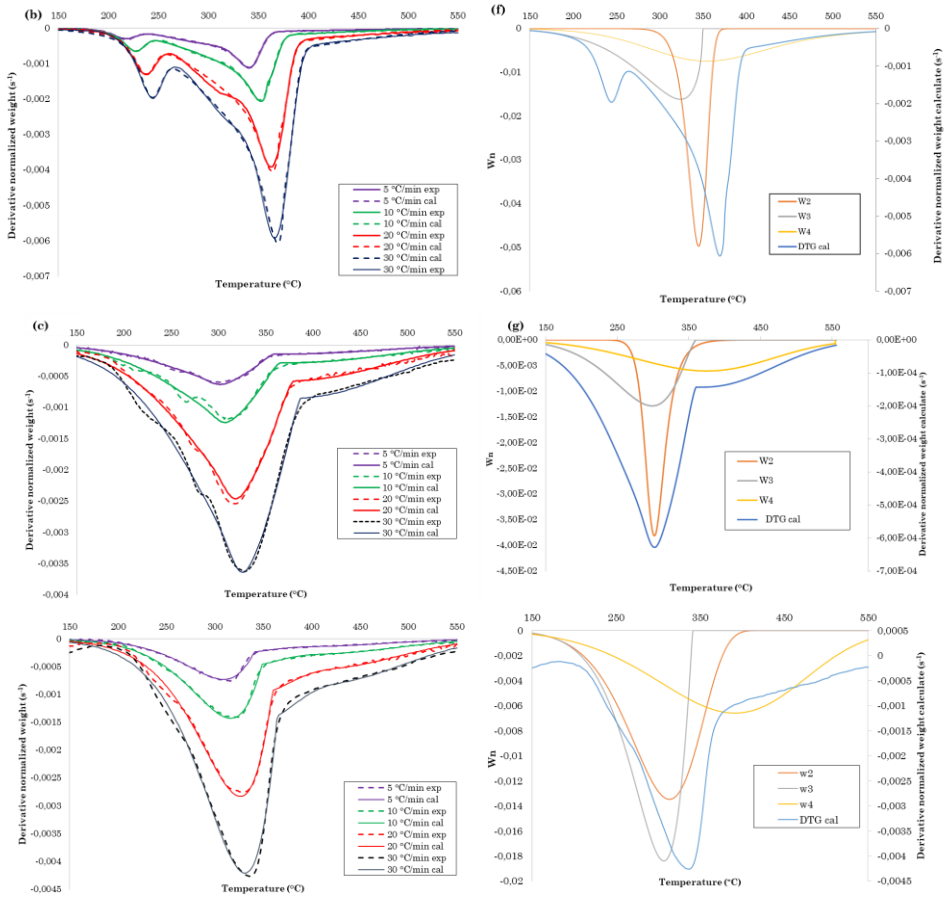

Fig. 2 (a–d) Experimental and calculated DTG curves for balsa wood, sugarcane bagasse, cocoa husk, and coffee husk at heating rates of 5, 10, 20, and 30 °C·min^{-1}; (e–h) deconvolution of pseudo-component contributions (W_1–W_4) derived from the Independent Parallel Reaction (IPR) model.

Table 5
Quantification of cellulose, hemicellulose, and lignin in cocoa husk and shell waste

	% Hemicellulose	% Cellulose	% Lignin
Bl	28.68	33.72	37.60
Bg	31.50	35.30	33.30
Cc	31.89	25.75	42.36
Cf	29.40	23.10	47.50

decomposition occurring between 190–320 °C. The higher-energy stages (W_3–W_4 ≈ 200–214 kJ·mol^{-1}) correspond to cellulosic degradation, responsible for the main weight loss peak, as similarly observed by (Najafi, Sani, & Sobati , 2024). The uniformity of n values (0.4–4.2) indicates mixed-order kinetics, with both depolymerization and fragmentation pathways active in the thermal breakdown.

For Cc y Cf, characterized by higher lignin contents (42.36% and 47.50%, respectively), displayed different kinetic profiles. For Cocoa husks, the initial decomposition steps (W_3, W_4) showed very low activation energies (31–44 kJ mol^{-1}), attributed to the volatilization of low-molecular-weight extractives and non-structural components, which are abundant in cocoa shells. The main decomposition step (W_2) presented an Ea of 323.9 kJ mol^{-1}, reflecting the thermal stability provided by the high lignin content and its interaction with cellulose. Coffee husks exhibited a more complex behavior with high Ea values across multiple components (W_1 to W_3 ranging from 898 to 1172 kJ mol^{-1}), suggesting a highly recalcitrant structure, possibly due to the presence of inorganic compounds or strong lignocellulosic matrix interactions that hinder thermal degradation. Similar multimodal behaviors were reported by (Escalante, y otros, 2022) and (Siddiqi H. &., 2020) for lignin-rich biomasses exhibiting strong intercomponent interactions.

Activation energies obtained for balsa were 73–468 kJ mol^{-1}, while cocoa husk exhibited values of 31–324 kJ mol^{-1},=confirming higher reactivity of the latter due to its greater volatile content and lower structural). These ranges agree with those reported by (Siddiqi H. &., 2020) for coconut shell (78–145 kJ mol^{-1}) and by (El-Sayed & Khairy, 2015) for cereal residues (80–190 kJ mol^{-1}).

Overall, the observed E_a values fall within the typical literature ranges 70–150 kJ·mol^{-1} for hemicellulose, 150–250 kJ·mol^{-1} for cellulose, and 200–400 kJ·mol^{-1} for lignin (Yang H. &., 2007). The fitting results demonstrated a high degree of accuracy, with residual errors below 7% for TG and 5% for DTG curves across all heating rates. This confirms that the IPR model effectively captures the multi-step degradation nature of these heterogeneous biomasses. The pre-exponential factors k_0 varied significantly (10^3–10^{38} s^{-1}), a variation that is consistent with the Kinetic Compensation Effect (KCE) often observed in biomass pyrolysis (Siddiqi H. &., 2020). This effect implies that an increase in activation energy is mathematically compensated by an increase in the pre-exponential factor, maintaining the reaction rate constant at the isokinetic temperature evidences the kinetic compensation effect, commonly reported in biomass pyrolysis (Siddiqi H. M., 2022).

Table 5 correlates these kinetic findings with the chemical composition. The high lignin content in Cc and Cf correlates with the broader decomposition temperature ranges and the complex kinetic parameters observed, reinforcing the role of lignin as a thermal stabilizer that promotes char formation over volatile release. In contrast, the kinetic profiles of Bl and Bg are more characteristic of holocellulose dominated decomposition, favoring sharp volatilization steps ideal for bio-oil or syngas production

Despite certain differences observed in elemental composition and moisture content, the most significant distinctions among these biomasses are found in their cellulose, hemicellulose, and lignin distributions. Literature data indicate that balsa wood and bagasse are richer in cellulose (40–45%) and present more balanced proportions of hemicellulose (23–

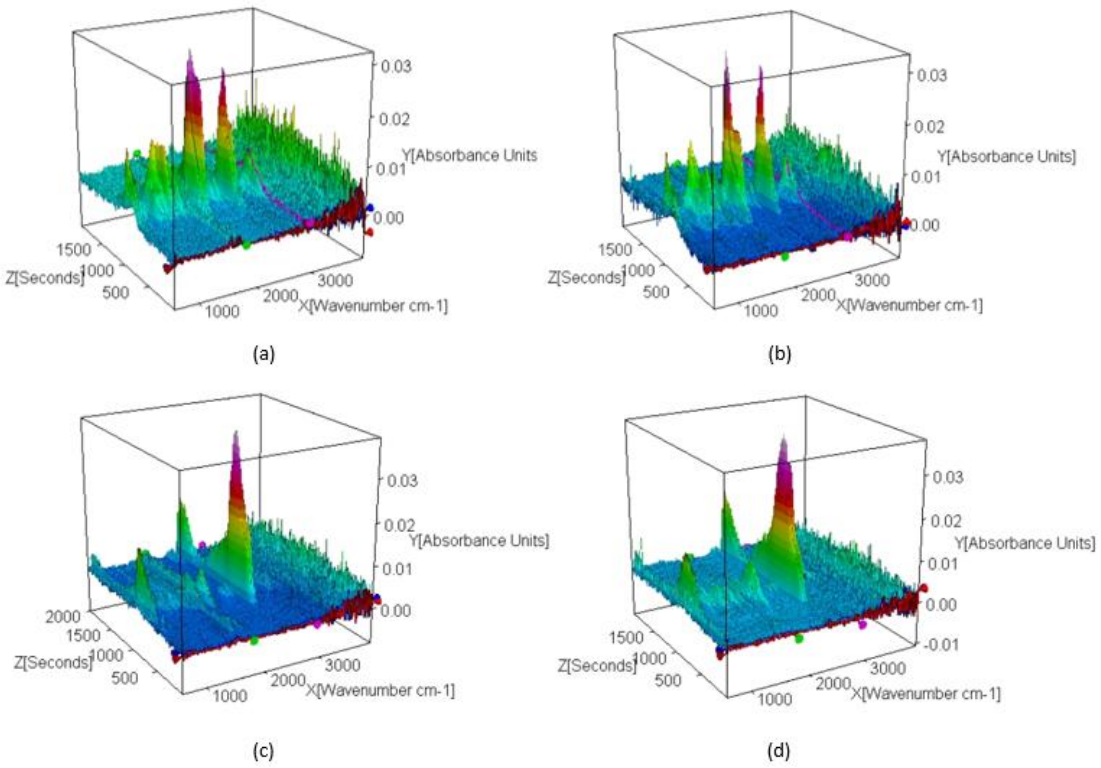

Fig. 3 Three-dimensional spectra of TG-FTIR of balsa wood (Bl), sugarcane bagasse (Bg), cocoa husk (Cc) and coffee husk (Cf).

27%) and lignin (20–25%) (Raveendran, Pyrolysis characteristics of biomass and biomass components, 1996) (Soares, 2020) (Ouensanga & Picard, 1988). Conversely, cocoa and coffee husks show more heterogeneous compositions: cellulose contents range from 19–35%, hemicellulose from 9–22% for cocoa and 24–45% for coffee, and lignin between 14–44% for cocoa and 18–30% for coffee (Reis, 2020) (Changjuna, 2014), cocoa husk, in particular, also contains significant extractive fractions such as pectin (Aleida, 2018).

The comparative interpretation suggests that cellulosic biomasses (balsa, bagasse) exhibit sharper DTG peaks and lower char residues, indicative of dominant devolatilization reactions, whereas lignin-rich residues decompose more gradually, producing broader peaks and higher solid yields. These results confirm the relationship between the macromolecular composition and thermal reactivity, as observed in the alkaline-catalyzed bagasse study by (Munoz, 2024). To ensure that peak positions/heights (DTG) and overall mass balance (TG) are simultaneously reproduced. A small global correction factor β was used per heating rate to absorb instrumental/sample dispersion without altering the physical meaning of the kinetic parameters. Improved the overlap between experimental and calculated DTG peaks (Table 2). These results are consistent with other studies using IPR or Distributed Activation Energy Models for biomass, confirming that the decomposition of each pseudo-component follows first-order or fractional-order kinetics (Yang H. &., 2007; Biagini, 2006).

3.4. Evolution of gaseous species (FTIR)

Real-time monitoring of evolved volatiles was performed to correlate the mass loss events observed in TGA with specific chemical functionalities. The coupling of thermogravimetry with infrared spectroscopy allows for the "fingerprinting" of decomposition products, providing essential data on the impact of biomass pretreatment and composition on pyrolytic pathways (El-Azazy, 2022) (Carrillo, 2004).

The volatile stream from the thermogravimetric analysis (TGA) was directly coupled to the infrared spectrometer for real-time detection. Figure 3 presents three-dimensional spectra of the volatiles from balsa wood, sugarcane bagasse, cocoa hulls, and coffee husk, which map the intensity of infrared absorbance against temperature and wavenumber. The 3D profiles reveal that the maximum evolution of volatiles occurs in the temperature range of 320–360 °C for Bl and Bg, coinciding with the maximum degradation rate DTG_{max} of cellulose determined in the kinetic study. In contrast, Cc and Cf exhibit a broader volatile release window starting at lower temperatures (~280 °C), consistent with their higher hemicellulose and extractives content

To identify specific functional groups, the 2D FTIR spectra were extracted at the temperatures of maximum volatile emission (Figure 4). The assignments of the main absorption bands are summarized in. Table 6. A broad absorption band between 3600–3200 cm^{-1}, corresponding to the O–H stretching vibration of water, was detected in all samples, with higher intensity for balsa wood and coffee hulls. Weak absorptions in the 3100–3000 cm^{-1} range, related to C–H stretching in aromatics and heterocycles (such as furan and furfural), were observed predominantly in the coffee hulls, although they could be masked by the broad O–H stretching band (Alghooneh, 2017).

The bands between 3000–2800 cm^{-1} are associated with C–H stretching of aliphatic compounds (alkanes), particularly notable in balsa wood and sugarcane bagasse. Peaks at 2349–2300 cm^{-1}, attributed to asymmetric stretching of CO_2, and 2180–2100 cm^{-1}, attributed to CO stretching, were more intense in cocoa and coffee samples, indicating greater production of simple gases during pyrolysis. Absorptions around 1730–1700 cm^{-1}, linked to carbonyl groups (C=O) from aldehydes, ketones, and carboxylic acids (Bilba, 1996), were weaker in cocoa and coffee hulls, suggesting differences in cellulose, hemicellulose, and lignin content between the biomasses. Bands between 1510–1490 cm^{-1} are attributed to aromatic skeletal C=C–C vibrations, while absorptions around 1470–1450 cm^{-1} correspond to methyl ($-CH_3$) and methylene ($-CH_2$) group bending, indicators of lignin degradation (Hergert, 1960). Signals between 1300–1120 cm^{-1} and 1260–1230 cm^{-1} represent C–O stretching vibrations, associated with ethers and esters. Finally, the 1150–1050 cm^{-1} region is characteristic of C–OH stretching in primary, secondary, and tertiary alcohols,

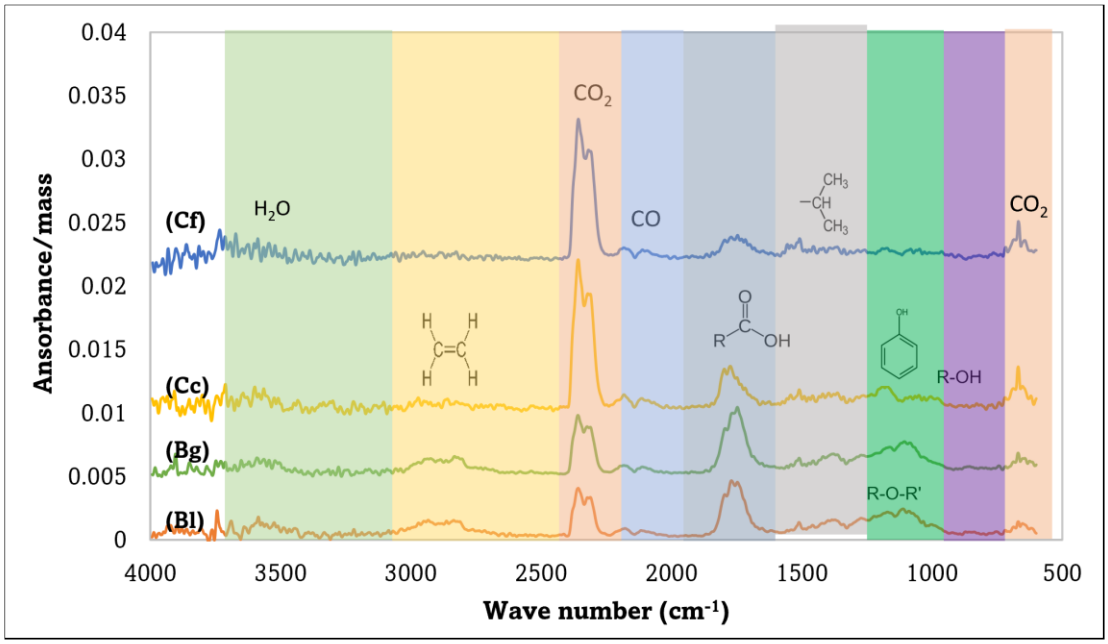

Fig. 4 FTIR spectra of volatile products evolved during pyrolysis of balsa wood (Bl), sugarcane bagasse (Bg), cocoa husk (Cc) and coffee husk (Cf).

Table 6
Summary of functional groups and identified chemical species of biomass residues

Wavenumber (cm^{-1})	Origin	Assignment	Bl (350 °C)	Bg (350 °C)	Cc (280 °C)	Cf (280 °C)
3600–3200	Symmetric and asymmetric O–H stretching	Water (H_2O)	H	H	L	L
3100–3000	Aromatic C–H stretching	Aromatic hydrocarbons and heterocycles (furans, furfurals)	L	L	L	L
3000–2800	Aliphatic C–H stretching	Alkanes	H	H	L	L
2349–2300	Asymmetric O=C=O stretching	Carbon dioxide (CO_2)	M	M	H	H
2180–2100	CO stretching	Carbon monoxide (CO)	MH	MH	H	H
1850–1770	C=O stretching	Anhydrides	L	L	L	L
1730–1700	C=O stretching	Aldehydes, ketones, esters, and carboxylic acids	H	H	M	M
1670–1620	C=C stretching	Alkenes and benzene	H	H	M	M
1510–1490	Aromatic C=C–C ring stretching	Benzene nucleus	M	M	L	M
1470–1450	Asymmetric C–H bending ($–CH_3$, $–CH_2$)	Alkanes	L	L	L	L
1300–1120	C–O stretching	Dialkyl ethers (R–O–R)	L	L	L	L
1260–1230	Symmetric and asymmetric C–O stretching	Esters and anhydrides	L	L	L	L
1200–1140	COOH group stretching and torsion	Carboxylic acids	M	M	L	L
1150–1050	C–OH stretching vibrations	Primary, secondary, and tertiary alcohols	L	L	L	L

Note: The relative intensity of each functional group absorption was qualitatively classified as High (H), Medium (M), or Low (L) according to the strength of the FTIR signal at the corresponding wavenumber for each biomass sample.

suggesting the presence of residual polysaccharides or lignin fragments (Sierra, 2009).

3.5. Pyrolysis products identified by Py–GC/MS

Analytical pyrolysis (Py-GC/MS) enabled the molecular characterization of the volatile fraction generated between 250 and 850 °C. This technique provided semi-quantitative fingerprints of the condensable vapors and supported the reaction pathways inferred from TGA/DTG and TG–FTIR analyses. A total of 134, 236, 111 and 103 compounds were identified for balsa wood, sugarcane bagasse, cocoa husks and coffee husks, respectively, using a similarity match >80%. The compounds were classified into acids, alcohols, aldehydes, ketones, phenols, esters, furans, hydrocarbons, and nitrogen-containing species, consistent with previously reported methodologies (Leng, 2023) (Muñoz, 2024) (Siddiqi H. M., 2022) (Ansari, 2021).

The chromatograms (Figure 5) show that all biomasses exhibited an increasing number of peaks with temperature up to 450–550 °C, the same region where DTG curves displayed maximum mass-loss rates, confirming that the most intense volatilization corresponds to holocellulose decomposition. Above 650 °C, the decline in peak abundance reflects secondary cracking and the formation of low-molecular-weight gases, which is consistent with the dominant CO_2 and CO absorption bands observed in FTIR (Pielsticker, 2021).

For Bl, the chromatograms showed limited volatile release at 250 and 350 °C, with the major production occurring at 450 and 550 °C. Predominant groups included alcohols, aldehydes, phenols, organic acids, and saturated hydrocarbons. Above 650 °C, the quantity of detectable volatile compounds progressively decreased, with a relative increase in aromatic hydrocarbons and carbon dioxide, indicating further cracking and condensation reactions (Figure 4a). The identified volatiles were mainly derived from the degradation of cellulose and hemicellulose, such as furfural, hydroxyacetaldehyde, acetic acid, and 2-furanmethanol, in agreement with previous studies (Lu, 2016) (Yang Z. &., 2019) (Xing, 2011) (Aho, 2008).

For Bg, the chromatographic profile was similar to that of balsa wood (Figure 4b). The maximum volatile generation was observed between 450 °C and 550 °C, dominated by organic acids, phenols, aldehydes, and saturated hydrocarbons. The most abundant compounds included acetic acid, furfural, and various phenolic derivatives such as 2-methoxyphenol and 2,6-dimethoxyphenol, corroborating results from similar lignocellulosic studies (Kumar, 2022; Muñoz, 2024). At temperatures above 650 °C, the bagasse exhibited a shift towards lighter compounds and increased CO_2 production, confirming the occurrence of secondary cracking.

In contrast, Cc displayed a distinctly different pyrolytic behavior (Figure 5c). The chromatograms showed a sharp maximum in the number of peaks at 450 °C, followed by a pronounced reduction at higher temperatures. The relative abundance of alcohol and organic acids was notable at intermediate temperatures, while at 850 °C, there was a significant increase in the proportion of aromatic hydrocarbons such as benzene, toluene, styrene, and naphthalene (Mansur, 2014). This behavior reflects the lower lignocellulosic polymer content in cocoa hulls compared to balsa and bagasse, leading to earlier degradation and volatilization of lighter compounds.

Finally, Cf presented the lowest intensity and number of volatile peaks among the studied materials (Figure 5d). The chromatograms indicated that CO_2 was the dominant compound at all temperatures, with only minor contributions from alcohols, saturated hydrocarbons, and nitrogenous compounds such as caffeine (Wan, y otros, 2024; Arun P & Muraleedharan , 2025). At 450 °C, coffee husks exhibited moderate production of aldehydes (hydroxyacetaldehyde and propanal) and phenolic derivatives (e.g., 2-methoxyphenol), although at substantially lower levels than the other biomasses. As the temperature increased, caffeine was detected

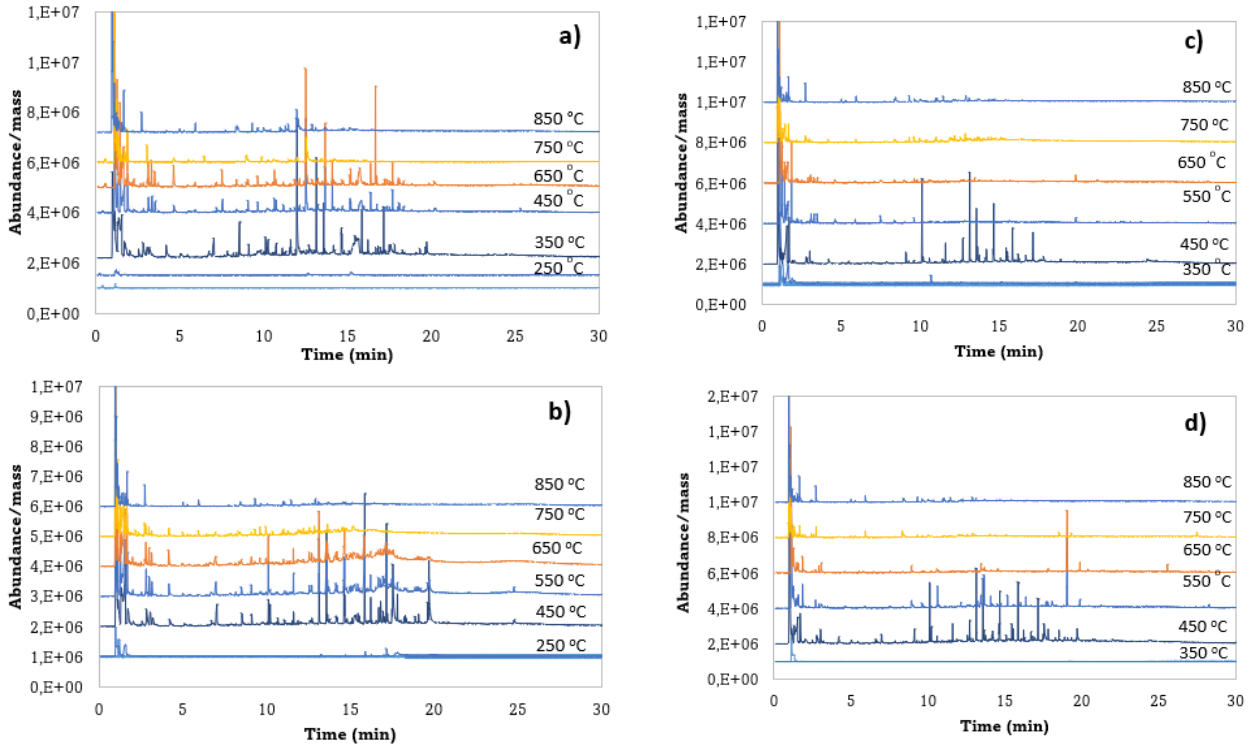

Fig. 5 Chromatograms of waste of balsa wood (Bl), sugarcane bagasse (Bg), cocoa husk (Cc) and coffee husk (Cf).

predominantly between 550 and 750 °C, confirming its thermal stability relative to other biomass components (Varma, 2017) (Jackels, 2014) (Fardhyantil, 2019).

The relative abundances displayed in Figure 6 indicate that balsa and bagasse produce a broader range of oxygenated compounds characteristic of cellulose and hemicellulose pyrolysis, whereas cocoa and coffee husks yield higher proportions of phenols, aromatics and CO_2, consistent with their higher lignin content. These trends correlate strongly with kinetic parameters: holocellulosic biomasses exhibit lower activation energies in the main devolatilization stage and produce abundant primary oxygenates, while lignin-rich biomasses display higher activation energies and generate more phenolic and aromatic compounds.

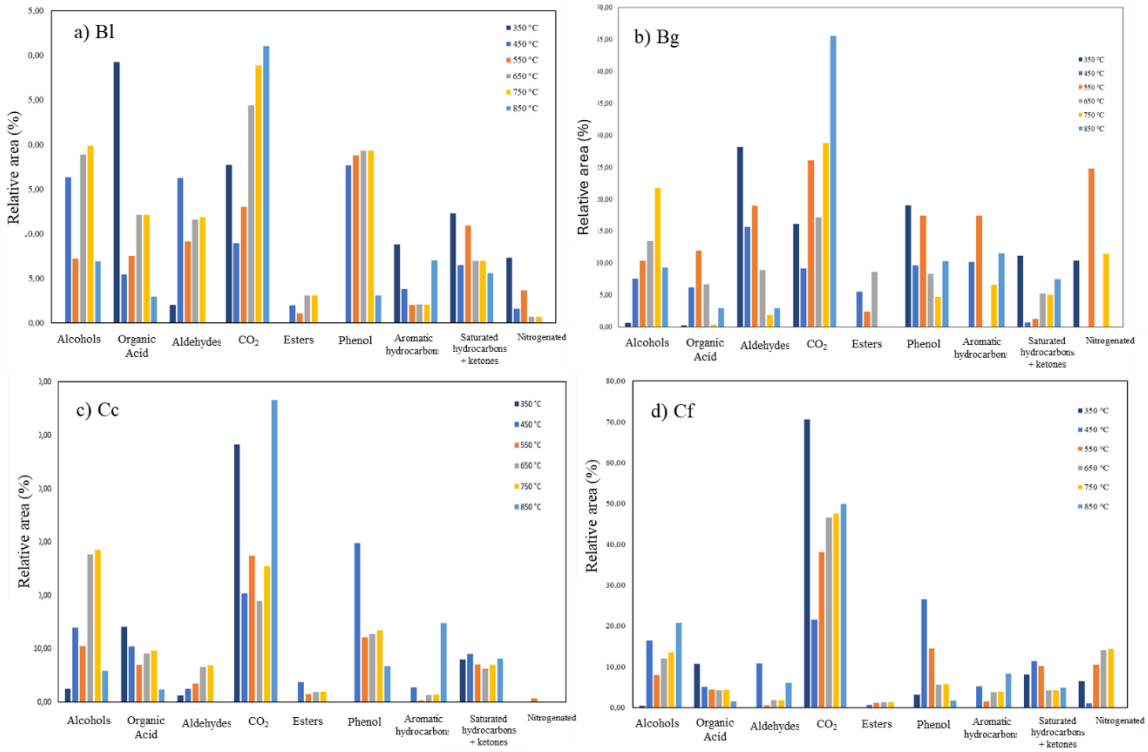

Fig. 6 Relative abundance of the main classes of volatile compounds at different temperatures for (a) balsa residues, (b) sugarcane bagasse, (c) cocoa husk and (d) coffee husk.

Figure 6 presents a comparative diagram between the classes of chemical compounds for the different biomasses at 450 °C, it is observed that for the balsa wood it has a higher percentage of alcohols, and saturated hydrocarbons. The bagasse sugarcane sample has a higher percentage of organic acids, esters, and aromatic hydrocarbons. Coffee has a higher percentage of carbon dioxide and caffeine which is a nitrogenous compound that increases with temperature response reaching its maximum 750 °C.

According to the analysis, balsa wood (Figure 6a) exhibits the highest relative areas for alcohols and aldehydes compared to the other biomasses. This behavior is consistent with the decomposition pathways of cellulose and hemicellulose, where primary and secondary alcohols are among the main products. In addition, a considerable proportion of phenolic compounds are observed at intermediate and high temperatures, reflecting the thermal degradation of lignin fractions. For coffee husks (Figure 6d), the results reveal the greatest production of saturated hydrocarbons and ketones, along with significant proportions of alcohols and phenols. The behavior observed for coffee husks closely resembles that of balsa wood in terms of alcohol production, and that of cocoa hulls in terms of phenolic compound formation. Additionally, coffee husks exhibit a consistent and elevated generation of carbon dioxide (CO_2) across all temperatures tested, alongside the detection of specific nitrogenous compounds such as caffeine, particularly between 550 °C and 750 °C.

The analysis also shows that both cocoa hulls and coffee husks generate a higher proportion of CO_2 compared to balsa wood and sugarcane bagasse. This finding correlates with the lower thermal stability and higher oxygen content of these two residues, which promote the early release of CO_2 during pyrolysis. The volatile compounds identified are of great industrial relevance due to their chemical properties. Organic acids, such as formic and acetic acids, are widely used as preservatives, disinfectants, and intermediates in the food, chemical, and pharmaceutical industries (Transparency Market Research, 2022; Ceylan, 2023; All About Feed, 2022). Aldehydes and ketones like acetaldehyde, propanal, and 2-propanone serve as raw materials to produce resins, solvents, and pharmaceuticals (Rice University, 2022). Moreover, glycerol derivatives such as glycidol have applications in the synthesis of epoxy resins and in bio-refinery processes (Prete, 2022) (Ricciardi, 2017).

Compounds like ethyl acetate, 1,2,4-trimethoxybenzene, and benzofuran are valued for their role in flavor and fragrance industries. Phenolic compounds such as vanillin are extensively used for the manufacture of plastics, resins, pharmaceuticals, and natural preservatives, owing to their antioxidant properties (Kumar, 2022) (P. Rathee, 2023). The 66 main peaks were identified, and the results are presented in Table 7, the different biomass gave similar chemical compounds, but with different proportions. The main compounds identified belong to oxygenated compounds, saturated and aromatic hydrocarbons and in low concentrations nitrogenous compounds, esters, and ethers. Oxygenated compounds included organic acid, aldehydes, ketones, and phenols. CO_2 being the highest percentage with respect to the other components. The compounds that had a higher percentage area were acetic acid, propanal, 1,2-Cyclopentanedione, 2-Methoxy-4-vinylphenol and Phenol, 2,6-dimethoxy.

The compositional differences observed between the biomasses underline the diversity and complexity of their chemical structures, influencing their potential applications in industrial and biotechnological processes. Balsa residues are characterized by a high proportion of alcohol and aldehydes, cocoa hulls by carboxylic acids and phenolic derivatives, and coffee husks by saturated hydrocarbons and ketones. These specific compositions position each biomass as a potential raw material for different value-added chemical production chains.

Pyrolysis and FTIR analyses confirmed the generation of typical lignocellulosic volatiles, with CO_2 and phenols predominating in cocoa and coffee residues, while aldehydes were more abundant in balsa and bagasse. Relevant compounds such as acetic acid, 2-methoxy-4-vinylphenol, and caffeine were identified, highlighting their potential for energy and chemical valorization.

Overall, the findings demonstrate that lignocellulosic composition strongly influences decomposition pathways and volatile product distribution, providing valuable insights for optimizing pyrolysis processes aimed at renewable energy generation and the recovery of value-added chemicals from agro-industrial residues. Future research should focus on kinetic modeling of pyrolytic reactions, scaling up flash pyrolysis systems under controlled conditions, and integrating catalytic upgrading to enhance yields of target compounds. These efforts will strengthen the role of biomass pyrolysis as a viable strategy for sustainable waste management and the development of circular bioeconomy models.

3.6. Kinetic and Chromatographic Correlations: Mechanistic Insights

The combined interpretation of kinetic parameters (TGA/IPR model) and molecular-level product distribution (Py–GC/MS) grants multiscale insights into the pyrolytic behavior of the four Ecuadorian biomasses. This approach aligns with advanced methodologies recommended in kinetic-pyrolysis literature, where correlations between devolatilization energy barriers and gas/liquid product speciation provide predictive understanding of biomass conversion pathways (Radmanesh, 2006).

A clear and systematic correlation was identified between the activation energy (Ea) associated with the main devolatilization stages (W_2, W_3) and the families of volatile compounds released during pyrolysis, as determined through Py–GC/MS. This relationship demonstrates that the chemical architecture of each biomass governs both the energetic requirements for thermal decomposition and the selectivity of the resulting vapors.

Holocellulosic biomasses, specifically balsa wood and sugarcane bagasse, exhibited moderate activation energies (129–241 $kJ{\cdot}mol^{-1}$), consistent with thermally induced depolymerization of cellulose and hemicellulose. These values correspond to glycosidic bond cleavage through concerted reactions requiring intermediate energy levels, in agreement with classical models of polysaccharide pyrolysis (Wang & Wu, 2023; Yang H. &., 2007). Their chromatographic profiles confirmed this interpretation: levoglucosan, anhydrosugars, furfural, 5-HMF, and light oxygenates such as acetic acid and hydroxyacetone were the predominant species. These results were supported by FTIR gas-phase spectra, which displayed strong carbonyl stretching bands around 1730 cm^{-1}, characteristic of aldehydes and ketones derived from dehydrated carbohydrate intermediates. Correspondingly, both biomasses exhibited sharp DTG peaks, indicative of a volatilization-controlled decomposition regime and minimal secondary cracking.

In contrast, cocoa and coffee husk (Cf) presented higher or more complex Ea values, reaching up to 323 $kJ{\cdot}mol^{-1}$ in the case of cocoa husk. These elevated energy barriers reflect the structural complexity and recalcitrance of lignin, whose degradation involves competitive radical reactions and progressive aromatic rearrangements. The DTG profiles of both biomasses displayed broad shoulders between 400 and 500 °C,

typical of overlapping lignin transformations. Their volatile fraction was enriched in methoxyphenols (guaiacol, syringol) and deoxygenated phenolic compounds formed through demethoxylation pathways. FTIR spectra revealed intense CO and CO_2 bands, indicating extensive decarboxylation and fragmentation reactions associated with the breakdown of lignin subunits. Coffee husk additionally released nitrogen-containing aromatics derived from caffeine decomposition, consistent with its higher nitrogen content. These findings align with established lignin pyrolysis mechanisms involving β-O-4 ether cleavage, radical recombination, and cross-linking (Biagini, 2006; Ríos, 2013).

For holocellulose-rich materials (Bl and Bg), decomposition primarily proceeded through rapid depolymerization of cellulose and hemicellulose. The process began with dehydration, forming levoglucosan and xylan-based

Table 7
List of the main decomposition products identified from pyrolysis for balsa, bagasse, cocoa and coffee residues. The table includes only the products corresponding to the relative abundance ≥ 0.5% for at least one of the samples.

				Relative area of identified compounds (%)			
No.	**Name**	**Formule**	**RT**	**Bl**	**Bg**	**Ca**	**Cc**
1	Carbon dioxide	CO_2	0.984	8.95	9.13	20.36	21.53
2	Formic acid, ethenyl ester	$C_3H_4O_2$	1.136	0.88	4.16	0.00	0.00
3	Glycidol	$C_3H_6O_2$	1.136	0.00	0.00	1.71	2.06
4	Acetic acid, methyl ester	$C_3H_6O_2$	1.196	0.00	0.00	1.41	0.00
5	Acetaldehyde, hydroxy-	$C_2H_4O_2$	1.333	3.78	3.65	0.66	3.12
6	Acetic acid ethenyl ester	$C_4H_6O_2$	1.34	0.00	0.00	0.87	0.00
7	Acetic acid	$C_2H_4O_2$	1.576	4.82	4.27	10.08	4.62
8	2-Propanone, 1-hydroxy-	$C_3H_6O_2$	1.72	0.97	2.68	2.75	3.20
9	Ethene, 1,1'-[1,2-ethanediylbis(oxy)]bis-	$C_6H_{10}O_2$	2.031	0.00	0.91	0.00	0.00
10	Propionoin	$C_6H_{12}O_2$	2.054	0.00	0.00	0.80	0.61
11	1-Penten-3-one	C_5H_8O	2.57	0.17	0.65	0.00	0.70
12	1-Hydroxy-2-butanone	$C_4H_8O_2$	2.775	0.00	0.00	0.50	0.00
13	2-Propanone, 1-hydroxy-	$C_3H_6O_2$	2.828	0.00	1.61	0.63	0.86
14	1,2-Ethanediol, monoacetate	$C_4H_8O_3$	2.836	0.94	0.00	0.00	0.00
15	Propanal	C_3H_6O	3.056	1.08	1.30	1.28	1.75
16	Propanoic acid, 2-oxo-, methyl ester	$C_4H_6O_3$	3.208	0.65	1.35	0.22	0.42
17	Pyrazole, 1,4-dimethyl-	$C_5H_8N_2$	4.202	0.00	0.00	1.13	0.00
18	Furfural	$C_5H_4O_2$	4.225	0.81	1.21	0.00	1.24
19	2-Furanmethanol	$C_5H_6O_2$	5.082	0.26	0.67	0.43	0.77
20	2-Propanone, 1-(acetyloxy)-	$C_5H_8O_3$	5.454	0.00	0.12	0.34	0.34
21	Ethanone, 1-(2-furanyl)-	$C_6H_6O_2$	6.638	0.00	0.00	0.00	0.55
22	1,2-Cyclopentanedione	$C_5H_6O_2$	7.033	1.67	1.74	1.05	1.05
23	Spiro[2.4]heptan-4-one	$C_7H_{10}O$	7.875	0.00	0.00	0.29	0.32
24	1-Decanol	$C_{10}H_{22}O$	7.898	0.17	0.36	0.00	0.22
25	Oxazolidine, 2,2-diethyl-3-methyl-	C_8H1_7NO	8.543	0.66	0.00	0.00	0.00
26	2-Methyliminoperhydro-1,3-oxazine	$C_5H_{10}N_2O$	8.566	0.00	1.82	0.00	0.00
27	1,2-Cyclopentanedione, 3-methyl-	$C_6H_8O_2$	9.12	0.45	0.46	1.09	1.12
28	2(3H)-Furanone, 5-hexyldihydro-	$C_{10}H_{18}O_2$	9.811	0.00	0.54	0.00	0.00
29	Phenol, 2-methoxy-	$C_7H_8O_2$	10.122	0.86	0.00	6.46	4.01
30	Pentanal	$C_5H_{10}O$	10.221	0.94	1.05	0.00	1.43
31	2-Cyclopenten-1-one, 3-ethyl-2-hydroxy-	$C_7H_{10}O_2$	10.6	0.00	0.00	0.34	0.26
32	2,4(3H,5H)-Furandione, 3-methyl-	$C_5H_6O_3$	10.752	0.00	0.54	0.00	0.00
33	1H-Azepine, hexahydro-1-nitroso-	$C_6H_{12}N_2O$	11.086	0.15	0.21	0.00	0.00
34	2(3H)-Furanone, 5-heptyldihydro-	$C_{11}H_{20}O_2$	11.131	0.19	0.15	0.00	0.00
35	2-Methoxy-5-methylphenol	$C_8H_{10}O_2$	11.617	0.40	0.54	1.67	0.97
36	Benzofuran, 2,3-dihydro-	C_8H_8O	11.989	0.00	6.30	0.00	0.00
37	1,2-Benzenediol, 3-methoxy-	$C_7H_8O_3$	12.566	0.00	0.00	0.00	0.38
38	Phenol, 4-ethyl-2-methoxy-	$C_9H_{12}O_2$	12.718	0.47	0.34	1.89	1.20

Table 7 (Cont'd)
List of the main decomposition products identified from pyrolysis for balsa, bagasse, cocoa and coffee residues. The table includes only the products corresponding to the relative abundance ≥ 0.5% for at least one of the samples.

				Relative area of identified compounds (%)			
No.	**Name**	**Formule**	**RT**	**Bl**	**Bg**	**Ca**	**Cc**
39	2-Methoxy-4-vinylphenol	$C_9H_{10}O_2$	13.143	1.59	2.83	6.18	4.35
40	Phenol, 2,6-dimethoxy-	$C_8H_{10}O_3$	13.583	2.89	1.43	3.67	4.11
41	Phenol, 2-methoxy-4-(2-propenyl)-	$C_{10}H_{12}O_2$	13.651	0.38	0.11	1.14	0.86
42	Benzenemethanol, .alpha.-ethyl-4-methoxy-	$C_{10}H_{14}O_2$	13.757	0.00	0.00	0.57	0.77
43	Vanillin	$C_8H_8O_3$	14.175	0.39	0.37	0.35	0.59
44	Vanillin lactoside	$C_{20}H_{28}O_{13}$	14.221	0.26	0.19	0.00	0.00
45	Phenol, 2-methoxy-4-(1-propenyl)-	$C_{10}H_{12}O_2$	14.213	0.00	0.00	0.95	0.92
46	1,2,4-Trimethoxybenzene	$C_9H_{12}O_3$	14.63	1.26	0.70	0.79	1.08
47	Phenol, 2-methoxy-4-(1-propenyl)-, (E)-	$C_{10}H_{12}O_2$	14.668	1.02	0.61	3.93	2.97
48	Benzene, 1-methoxy-4-[1-(methyl-d)propyl-1-d]-	$C_{11}H_{14}D_2O$	14.813	0.25	0.13	0.00	0.00
49	1,2-Benzenediol, 4-(1,1-dimethylethyl)-	$C_{10}H_{14}O_2$	15.109	0.23	0.13	0.72	0.72
50	Benzene, 1,2,3-trimethoxy-5-methyl-	$C_{10}H_{14}O_3$	15.458	0.00	0.00	0.78	1.12
51	2-Propanone, 1-(4-hydroxy-3-methoxyphenyl)-	$C_{10}H_{12}O_3$	15.541	0.00	0.00	0.85	0.94
52	Ethanone, 1-(3,4-dimethoxyphenyl)-	$C_{10}H_{12}O_3$	15.868	4.02	1.45	2.48	3.56
53	Phenol, 4-(3-hydroxy-1-propenyl)-2-methoxy-	$C_{10}H_{12}O_3$	16.11	0.16	0.14	0.00	0.00
54	Phenol, 2,6-dimethoxy-4-(2-propenyl)-	$C_{11}H_{14}O_3$	16.224	4.42	2.17	4.21	3.66
55	Benzaldehyde, 4-hydroxy-3,5-dimethoxy-	$C_9H_{10}O_4$	16.816	0.97	0.38	0.00	0.49
56	Phenacetic amide, 2-methoxy-6-nitroso-.alpha.,.alpha.-dimethyl-	$C_{11}H_{14}N_2O_3$	17.044	0.18	0.32	0.00	0.00
57	Ethanone, 1-(4-hydroxy-3,5-dimethoxyphenyl)-	$C_{10}H_{12}O_4$	17.492	0.40	0.21	0.00	0.44
58	4-((1E)-3-Hydroxy-1-propenyl)-2-methoxyphenol	$C_{10}H_{12}O_3$	17.552	4.78	0.42	0.56	3.19
59	2-Pentanone, 1-(2,4,6-trihydroxyphenyl)	$C_{11}H_{14}O_4$	18.236	0.20	0.27	0.00	0.93
60	Caffeine	$C_8H_{10}N_4O_2$	18.524	0.00	0.00	0.00	1.06
61	Phenol, 2-methoxy-4-(methoxymethyl)-	$C_9H_{12}O_3$	18.896	0.00	0.00	0.32	0.31
62	3,5-Dimethoxy-p-coumaric alcohol	$C_{11}H_{14}O_4$	19.086	0.40	0.14	0.00	0.00
63	Hexadecanoic acid	$C_{16}H_{32}O_2$	19.336	0.00	0.22	0.00	0.24
64	3,5-Dimethoxy-p-coumaric alcohol	$C_{11}H_{14}O_4$	19.7	4.58	0.84	0.00	1.68
65	Asarone	$C_{12}H_{16}O_3$	21.871	0.09	0.00	0.24	0.00
66	10,11-Dihydro-10-hydroxy-2,3-dimethoxydibenz(b,f)oxepin	$C_{16}H_{16}O_4$	24.383	0.00	0.00	0.74	0.24

RT – Retention time

intermediates, followed by ring-opening reactions that generated furans and small oxygenates. This pathway was validated by the strong FTIR carbonyl bands (1730 cm^{-1}), the marked presence of anhydrosugars and furanics in the GC/MS spectra, and the sharp DTG maxima, which reflect kinetically uniform depolymerization and limited influence of secondary reactions. The low ash content of both biomasses additionally reduced catalytic cracking, favoring primary pyrolytic products. The higher mineral content (notably K and Ca) in cocoa and coffee husks likely catalyzes secondary decarboxylation and charring reactions, as suggested by (Radmanesh, 2006; Pielsticker, 2021), contributing to reduced liquid yields and increased char stability.

Conversely, lignin-rich biomasses (Cc and Cf) followed a pathway dominated by aromatic bond scission and mineral-assisted transformations. The mechanism initiated with β-O-4 cleavage of lignin's phenylpropanoid units, generating methoxyphenols that subsequently underwent demethoxylation to form phenols and CO_2. The broad DTG region observed for these residues reflects the multistep, overlapping nature of lignin degradation. FTIR spectra were dominated by CO_2 bands at ~2350 cm^{-1}, reinforcing the prevalence of decarboxylation reactions. GC/MS analysis revealed a wide distribution of phenolic species, consistent with lignin depolymerization pathways (Liu, Wang, Zheng, Lou, & Cen, 2008).

Thus, the combined TGA, FTIR and Py-GC/MS results converge to a coherent view. Balsa wood and sugarcane bagasse, with their higher cellulose and lignin content, offered more complex volatile profiles suitable for bio-based chemical production like abundant furans, aldehydes, acids and alcohols, and high lignin generated intense phenolic/aromatic formation and elevated CO_2. In contrast, cocoa hulls and coffee husks, due to their lower polymeric content and higher thermal reactivity,

produced simpler profiles dominated by CO_2 and early volatiles and nitrogenous compounds.

4. Conclusion

Thermogravimetric analysis revealed clear differences in the thermal decomposition patterns of the lignocellulosic residues studied. In balsa wood and sugarcane bagasse, hemicellulose and cellulose degradation stages were clearly distinguished, whereas in cocoa husk and coffee husk both processes overlapped, reflecting higher structural complexity and lignin content. The combined use of TGA–FTIR and Py–GC/MS provided a multiscale interpretation linking lignocellulosic composition, apparent kinetic domains, and volatile product speciation. Holocellulose-rich biomasses such as balsa wood and sugarcane bagasse exhibited moderate activation energy ranges and sharp devolatilization stages, favoring the formation of oxygenated compounds including aldehydes, alcohols, furans, and organic acids. In contrast, cocoa and coffee husks, characterized by higher lignin content and mineral matter, displayed broader decomposition intervals, higher apparent activation energies, and volatile fractions dominated by phenolic compounds, aromatics, CO_2, and nitrogen-containing species. These results demonstrate that the chemical architecture of agro-industrial residues governs both the energetic barriers of thermal degradation and the selectivity of pyrolytic vapors. The integrated kinetic–molecular framework presented here provides a valuable basis for the selective valorization of Ecuadorian biomasses, supporting informed decisions on their suitability for bio-based chemical production or char-oriented thermochemical pathways.

Acknowledgments

Chemical Engineering Department of the University of Alicante, the Process Engineering Research Group (GiiP) of the Central University of Ecuador and the Institute of Geological and Energy Research of the Ministry of Energy of Ecuador (IIGE).

Author Contributions: M.R.E.: Conceptualization, data curation, formal analysis, writing—original draft preparation, review, and editing; M.M.B.: Conceptualization, methodology, data analysis, writing—original draft preparation, review, and editing; R.N.C.: Investigation, data collection, and writing—original draft preparation; S.E.: Investigation, validation, and writing—review and editing; B.G.S.: Investigation, validation, and writing—review and editing; Á.G.C.: Supervision, project administration, and writing—review and editing; A.M.: Supervision, resources, project administration, and writing—review and editing. All authors have read and agreed to the published version of the manuscript.

Funding: This research received no financial support for the research, authorship, and/or publication of this article.

Conflicts of Interest: The authors declare no conflict of interest.

References

Aho, A. K. (2008). Pyrolysis of softwood carbohydrates in a fluidized bed reactor. *Molecular Sciences, 9*(9), 1665-1675. https://doi.org/10.3390/ijms9091665

Aleida, J. S. (2018). Composition and Thermogravimetric Characterization of Components of Venezuelan Fermented and dry Trinitario Cocoa Beans (Theobroma cacao L.): Whole Beans, Peeled Beans and Shells. *Revista Técnica de la Facultad de Ingeniería Universidad del Zulia, 41*, 41-47. Retrieved from https://api.semanticscholar.org/CorpusID:196884814

Alghooneh, A. A. (2017). Characterization of cellulose from coffee silverskin. *Food Properties, 20*(11), 2830-2843. https://doi.org/10.1080/10942912.2016.1253097

Ansari, K. B. (2021). Recent developments in investigating reaction chemistry and transport effects in biomass fast pyrolysis: A review. *Renewable and Sustainable Energy Reviews, 150*, 111454. https://doi.org/10.1016/j.rser.2021.111454

Arun P, S., & Muraleedharan , C. (2025). Thermochemical conversion of coffee husk: a study on thermo-kinetic analysis, volatile composition and ash behavior. *Biomass Conv. Bioref, 15*, 20723–20740. https://doi.org/10.1007/s13399-025-06676-5

Bassilakis, R. &. (2001). TG-FTIR analysis of biomass pyrolysis. *Fuel*, 1765-1786. https://doi.org/10.1016/S0016-2361(01)00061-8

Biagini, E. &. (2006). Devolatilization of Biomass Fuels and Biomass Components Studied by TG/FTIR Technique. *Industrial & Engineering Chemistry Research, 45*(13), 4486–4493. https://doi.org/10.1021/ie0514049

Bilba, K. &. (1996). Fourier transform infrared spectroscopic study of thermal degradation of sugar cane bagasse. *ELSEVIER, 38*, 61-73. https://doi.org/10.1016/S0165-2370(96)00952-7

Carrillo, F. X. (2004). Structural FTIR analysis and thermal characterisation of lyocell and viscose-type fibres. *European Polymer Journal*, 2229-2234. https://doi.org/10.1016/j.eurpolymj.2004.05.003

Changjuna, L. W. (2014). Catalytic fast pyrolysis of lignocellulosic biomass. *Chemical Society Reviews, 43*(22), 7594 - 7623. https://doi.org/10.1039/c3cs60414d

Cutiño, E. M.-M. (2011). ANÁLISIS TERMOGRAVIMETRICO Y TÉRMICO. *Tecnología Química, 31*(2), 11.

de Lucas Herguedas, A., & Rodríguez García, E. (2012). *Biomasa, biocombustibles y sostenibilidad.* (E. Sanz González, & M. Sánchez Martín, Eds.) España: Instituto Universitario de Investigación en Gestión Forestal Sostenible. ISBN: 978-84-931891-5-0. https://www.researchgate.net/profile/Ana-De-Lucas/publication/260383181_Biomasa_biocombustibles_y_sostenibilidad/links/54201c510cf241a65a1b01e5/Biomasa-biocombustibles-y-sostenibilidad.pdf#:~:text=Esta%20publicaci%C3%B3n%20es%20el%20resultado,innovaci%C3%B3n%20aplicada%20y%20transferencia%20del

Dellarose, B. F.-M.-F. (2021). Pirólisis lenta del bagazo de caña de azúcar para la producción de carbón vegetal y el potencial de su subproducto para la protección de la madera. *Materiales Renovables, 9*(1), 97-117. https://doi.org/10.32604/jrm.2021.013147

Dhyani, V., & Bhaskar, T. (2019). Pyrolysis of Biomass. *Biomass, Biofuels, Biochemicals*, 217-244. https://doi.org/10.1016/B978-0-12-816856-1.00009-9

Dick, D. T. (2020). Pyrolysis of waste tyre for high-quality fuel products: A review. *AIMS Energy, 8*(5), 869–895. https://doi.org/10.3934/energy.2020.5.869

El-Azazy, M. A.-S.-S. (2022). Application of Infrared Spectroscopy in the Characterization of Lignocellulosic Biomasses Utilized in Wastewater Treatment. *Infrared Spectroscopy*. https://doi.org/10.5772/intechopen.108878

El-Sayed, S., & Khairy, M. (2015). Effect of heating rate on the chemical kinetics of different biomass pyrolysis materials. *6*(3-4), 157-170. https://doi.org/10.1080/17597269.2015.1065590

Escalante, J., Chen, W. H., Tabatabaei, M., Hoang, A., Kwon, E., Lin, K.-Y., & Saravanakumar, A. (2022). Pyrolysis of lignocellulosic, algal, plastic, and other biomass wastes for biofuel production and circular bioeconomy: A review of thermogravimetric analysis (TGA) approach. *Renewable and Sustainable Energy Reviews, 169*(1), 112914. https://doi.org/10.1016/j.rser.2022.112914

ESIN Consultora S.A. (2014). *Atlas Bioenergético del Ecuador* (primera ed.). Ecuador: ESIN Consultora S.A. Retrieved from https://www.mediafire.com/file/17dz5lbnwloiea6/ATLAS+BIOENERGETICO+DEL+ECUADOR.zip

Fagbemi, L. K. (2001). Pyrolysis products from different biomasses: application to the thermal cracking of tar. *Applied Energy, 69*(4), 293-306. https://doi.org/10.1016/S0306-2619(01)00013-7

Fardhyantil, D. S. (2019). Phenolic compound separation from bio-oil produced from pyrolysis of coffee shell at 700°C using liquid-liquid extraction. *Physics, 1444*(1), 1444. https://doi.org/10.1088/1742-6596/1444/1/012002

Garrido, M., Font, R., & Conesa, J. (2016). Kinetic study and thermal decomposition behavior of viscoelastic memory foam. *Energy Conversion and Management, 119*, 327-337. https://doi.org/10.1016/j.enconman.2016.04.048

Ge, X., Chang, C., Zhang, L., Cui, S., Luo, X., Hu, S., . . . Li, Y. (2018). Chapter Five - Conversion of Lignocellulosic Biomass Into Platform Chemicals for Biobased Polyurethane Application. *Advances in Bioenergy, 3*(1), 161-213. https://doi.org/10.1016/bs.aibe.2018.03.002

Gogoi, D. M. (2023). A Comprehensive Review on "Pyrolysis" for Energy Recovery. *BioEnergy Research*, 145–155. https://doi.org/10.1007/s12155-023-10568-9

Hergert, H. L. (1960). Infrared Spectra of Lignin and Related Compounds. II. Conifer Lignin and Model Compounds. *Organic Chemistry, 25*(3), 405–413. https://doi.org/10.1021/jo01073a026

Huertas, d. l. (2022). Pyrolysis-GC/MS, A Powerful Analytical Tool for Additives and Polymers Characterization. *Recent Perspectives in Pyrolysis Research*, 1-20. https://www.intechopen.com/chapters/80292

Jackels, S. C. (2014). GCMS Investigation of Volatile Compounds in Green Coffee Affected Green Coffee Affected. *Agricultutal and Food Chemestry, 62*(1), 10222−10229. https://doi.org/10.1021/jf5034416

Kumar, M. N. (2022). Pyrolysis of Sugarcane (Saccharum officinarum L.) Leaves and Characterization of Products. *ACS Omega, 7*(32), 28052–28064. https://doi.org/10.1021/acsomega.2c02076

Leng, E. H. (2023). Interactions between cellulose and lignin during pyrolysis: Evolutions of condensed-phase functional groups and gas-phase volatile fraction. *Industrial Crops and Products, 205*, 117518. https://doi.org/10.1016/j.indcrop.2023.117518

Li, B. W. (2014). Pyrolysis and catalytic pyrolysis of industrial lignins by TG-FTIR: Kinetics and products. *Analytical and Applied Pyrolysis*, 295-300. https://doi.org/10.1016/j.jaap.2014.04.002

Liu, Q. &. (2020). Mechanism study of wood lignin pyrolysis by using TG–FTIR analysis. *Analytical and Applied Pyrolysis, 82*(1), 170-177. https://doi.org/10.1016/j.jaap.2008.03.007

Liu, Q., Wang, S., Zheng, Y., Lou, Z., & Cen, K. (2008). Mechanism study of wood lignin pyrolysis by using TG–FTIR analysis. *Analytical and Applied Pyrolysis, 82*(1), 170-177. https://doi.org/10.1016/j.jaap.2008.03.007

Lu, Q. T.-y.-y.-q. (2016). Pyrolysis mechanism of holocellulose-based monosaccharides: The formation of hydroxyacetaldehyde. *Analytical and Applied Pyrolysis, 120*, 15-26. https://doi.org/10.1016/j.jaap.2016.04.003

Ma, M. X. (2014). Application of Pyrolysis Gas Chromatography/Mass Spectrometry in Lacquer Research: A Review. *Polymers*, 132-144.

Mahmuda, M. A. (2021). Sugarcane bagasse - A source of cellulosic fiber for diverse applications. *Heliyon, 7*(8), e07771. https://doi.org/10.1016/j.heliyon.2021.e07771

Manals, C. E.-M. (2018). Caracterización de la biomasa vegetal cascarilla de café. *Tecnología Química*, 8. https://tecnologiaquimica.uo.edu.cu/index.php/tq/article/view/3239/2869

Manals-Cutiño, E. y.-M.-T. (2015). Caracterización del bagazo de caña como biomada vegetal. *Tecnología Química, XXXV*(2), 179-192. Retrieved from https://www.redalyc.org/articulo.oa?id=445543787003

Mansur, D. &. (2014). Conversion of cacao pod husks by pyrolysis and catalytic reaction to produce useful chemicals. *Biomass and Bioenergy, 66*(1), 275-285. https://doi.org/10.1016/j.biombioe.2014.03.065

Molto, B. J. (2011). *Descomposición térmica de residuos textiles: estudio cinético y formación de contaminantes.* Alicante: Universidad de Alicante. https://rua.ua.es/server/api/core/bitstreams/6cde511e-feb2-4055-8839-78926e25da2e/content

Moncayoa, G. y.-M. (2018). Caracterización de las propiedades mecánicas de lamadera de balsa (Ochroma Pyramidale) Ecuatoriana. *Congreso de Ciencia y Tecnología ESPE*, 5. https://journal.espe.edu.ec/ojs/index.php/cienciaytecnologia/es/article/view/788

Munoz, M. &. (2024). Effect of alkaline catalysts on the valorization of sugarcane bagasse. *Industrial Crops and Products, 211*, 118225. https://doi.org/10.1016/j.indcrop.2024.118225

Muñoz, M. &. (2024). Effect of alkaline catalysts on the valorization of sugarcane bagasse via Pirolysis. *Industrial Crops & Products, 211*, 118225. https://doi.org/10.1016/j.indcrop.2024.118225

Najafi, H., Sani, A., & Sobati , M. (2024). Thermogravimetric and thermo-kinetic analysis of sugarcane bagasse pith: a comparative evaluation with other sugarcane residues. *Scientific Reports, 14*(1), 2076. https://doi.org/10.1038/s41598-024-52500-x

Ortiz de Bertorelli, L. (. (2004). Efecto del secado del sol sobre la calidad del grano fermentado de cacao. *Agronomía Tropical*, 1-12. https://ve.scielo.org/scielo.php?script=sci_arttext&pid=S0002-192X2004000100003

Ouedraogo, M. &. (2022). Characterization of sugar cane bagasse ash from Burkina Faso for cleaner. *Results in Materials, 14*, 100275. https://doi.org/10.1016/j.rinma.2022.100275

Ouensanga, A., & Picard, C. (1988). Thermal degradation of sugar cane bagasse. *Thermochimica Acta*, 89-97. https://doi.org/10.1016/0040-6031(88)87213-7

Rathee, R. S. (2023). Polyphenols: Natural Preservatives with Promising Applications in Food, Cosmetics and Pharma Industries; Problems and Toxicity Associated with Synthetic Preservatives; Impact of Misleading Advertisements; Recent Trends in Preservation and Legislation. *Materials, 16*, 4793. https://doi.org/10.3390/ma16134793

Patiño-Velasco, M. y.-F.-C. (2016). Determinación del contenido de humedad en granos de café pergamino seco utilizando SPECKLE DINÁMICO. *Biotecnología en el sector Agropecuario y Agroindustrial*, 84-91. https://doi.org/10.18684/BSAA(14)84-91

Pielsticker, S. G. (2021). Flash Pyrolysis Kinetics of Extracted Lignocellulosic Biomass Components. *Bioenergy and Biofuels, 9*, 737011. https://doi.org/10.3389/fenrg.2021.737011

Poyilil, S. &. (2022). Physico-chemical characterization study of coffee husk for feasibility assessment in fluidized bed gasification process. *Environmental Science and Pollution Research, 29*(1), 51041–51053. https://doi.org/10.1007/s11356-021-17048-7

Prete, P. &. (2022). Glycidol syntheses and valorizations: boosting the glycerol biorefinery. *Current Opinion in Green and Sustainable Chemistry, 35*, 100624. https://doi.org/10.1016/j.cogsc.2022.100624

Radmanesh, R. &. (2006). A unified lumped approach in kinetic modeling of biomass pyrolysis. *Fuel, 85*(9), 1211-1220. https://doi.org/10.1016/j.fuel.2005.11.021

Raveendran, K. A. (1996). Pyrolysis characteristics of biomass and biomass components. *Fuel*, 987-998.

Reed, T. B., & Siddhartha, G. (1994). Atlas of thermal data of biomass and other fuels—a report on the forthcoming book. *Biomass and Bioenergy, 1*(6), 143-145. https://doi.org/10.1016/0961-9534(94)00053-V

Reis, R. S. (2020). Characterization of coffee parchment and innovative steam explosion treatment to obtain microfibrillated cellulose as potential composite reinforcement. *Material Research and Technology, 9*(4), 9412-9421. https://doi.org/10.1016/j.jmrt.2020.05.099

Rezende, C. d. (2011). Chemical and morphological characterization of sugarcane bagasse submitted to a delignification process for enhanced enzymatic digestibility. *Biotechnology for Biofuels volume, 4*, 54. https://doi.org/10.1186/1754-6834-4-54

Ricciardi, M. &. (2017). Glycidol, a Valuable Substrate for the Synthesis of Monoalkyl Glyceryl Ethers: A Simplified Life Cycle Approach. *ChemSusChem, 10*(10), 2291-2300. https://doi.org/10.1002/cssc.201700525.

Ríos, F. M. (2013). *Modelización de procesos degradativos a partir de datos termogravimétricos.* Coruña: Universidad de Coruña. https://dialnet.unirioja.es/servlet/tesis?codigo=39633

Salazar, H. A.-H.-H., & Aburto, J. (2015). Principales componentes químicos de la madera de Ceiba pentandra, Hevea brasiliensis y Ochroma pyramidale. *Scielo*, 131-146. https://doi.org/10.21829/myb.2015.212450

Saldarriaga, J., Aguado, R., Pablos, A., Amutio, M., Olazar, M., & Bilbao, J. (2015). Fast characterization of biomass fuels by thermogravimetric analysis (TGA). *Fuel, 140*(15), 744-751. https://doi.org/10.1016/j.fuel.2014.10.024

Sangronis, E. S. (2014). Cascarilla de cacao venezolano como materia prima de infusiones. *ALAN, 64*(2), 123-130. https://ve.scielo.org/scielo.php?pid=S0004-06222014000200007&script=sci_abstract

Siddiqi, H. &. (2020). A synergistic study of reaction kinetics and heat transfer with multi-component modelling approach for the pyrolysis of biomass waste. *Energy, 204*(1), 117933. https://doi.org/10.1016/j.energy.2020.117933

Siddiqi, H. M. (2022). In-situ and ex-situ co-pyrolysis studies of waste biomass with spent motor oil: Elucidating the role of physical inhibition and mixing ratio to enhance fuel quality. *Bioresource Technology, 358*, 127364. https://doi.org/10.1016/j.biortech.2022.127364

Sierra, A. I. (2009). *Análisis Instrumental.* La Coruña-España: Netbiblo.

Soares, A. P. (2020). Thermal evaluation of composites from cofee capsules residue with sugarcane bagasse by TG/DTA and DMA. *Thermal Analysis and Calorimetry*. 142(4):1-10 https://doi.org/10.1007/s10973-020-10012-6

TranVan, L. &. (2014). Thermal decomposition kinetics of balsa wood: Kinetics and degradation mechanisms comparison between dry and moisturized materials. *Polymer Degradation and Stability, 110*(1), 208 - 215. https://doi.org/10.1016/j.polymdegradstab.2014.09.004

Varma, A. K. (2017). Pyrolysis of sugarcane bagasse in semi batch reactor: Effects of process parameters on product yields and characterization of products. *Industrial Crops and Products*, 704-717. https://doi.org/10.1016/j.indcrop.2016.11.039

Wan, L., Wang, H., Mo, X., Wang, Y., Song, L., Liu, L., & Liang, W. (2024). Applying HS-SPME-GC-MS combined with PTR-TOF-MS to analyze the volatile compounds in coffee husks of Coffea arabica with different primary processing treatments in Yunnan. *LWY, 191*(1), 115675. https://doi.org/10.1016/j.lwt.2023.115675

Wang, G. Y. (2020). A Review of Recent Advances in Biomass Pyrolysis. *Energy Fuels, 34*(12), 15557–15578. https://doi.org/10.1021/acs.energyfuels.0c03107

Wang, Y., & Wu, J. J. (2023). Thermochemical conversion of biomass: Potential future prospects. *Renewable and Sustainable Energy Reviews, 187*, 113754. https://doi.org/10.1016/j.rser.2023.113754

White, J. E. (2011). Biomass pyrolysis kinetics: A comparative critical review with relevant agricultural residue case studies. *Journal of Analytical and Applied Pyrolysis, 91*(1), 1-33. https://doi.org/10.1016/j.jaap.2011.01.004

Xing, R. &. (2011). roduction of furfural and carboxylic acids from waste aqueous hemicellulose solutions from the pulp and paper and cellulosic ethanol industries. *Energy & Environmental Science, 6*. https://doi.org/10.1039/C1EE01022K

Yang, H. &. (2007). Characteristics of hemicellulose, cellulose and lignin pyrolysis. *Fuel*, 1781-1788. https://doi.org/10.1016/j.fuel.2006.12.013

Yang, Z. &. (2019). Thermal Characteristics and Kinetics of Waste Camellia oleifera Shells by TG–GC/MS. *ACS Omega, 4*(6), 10370–10375. https://doi.org/10.1021/acsomega.9b01013

© 2026. The Author(s). This article is an open access article distributed under the terms and conditions of the Creative Commons Attribution-ShareAlike 4.0 (CC BY-SA) International License (http://creativecommons.org/licenses/by-sa/4.0/)